NASA TN D-1236

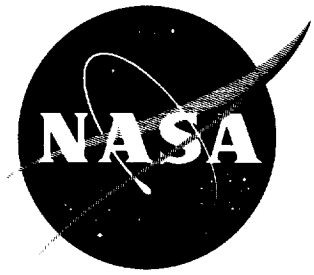

TECHNICAL NOTE

D-1236

EXPERIMENTAL INVESTIGATION OF OSCILLATORY AERODYNAMIC FORCES, MOMENTS, AND PRESSURES ACTING ON A TAPERED WING OSCILLATING IN PITCH AT MACH NUMBERS FROM 0.40 TO 1.07

By Sumner A. Leadbetter, Sherman A. Clevenson, and William B. Igoe

Langley Research Center
Langley Station, Hampton, Va.

NATIONAL AERONAUTICS AND SPACE ADMINISTRATION
WASHINGTON
April 1962

NATIONAL AERONAUTICS AND SPACE ADMINISTRATION

TECHNICAL NOTE D-1236

EXPERIMENTAL INVESTIGATION OF OSCILLATORY AERODYNAMIC FORCES, MOMENTS, AND PRESSURES ACTING ON A TAPERED WING OSCILLATING IN PITCH AT MACH NUMBERS FROM 0.40 TO 1.07

By Sumner A. Leadbetter, Sherman A. Clevenson, and William B. Igoe

SUMMARY

Aerodynamic forces, moments, and pressures, and their respective phase angles, associated with a deformed pitching mode oscillation of a wing having an aspect ratio of 3 and a taper ratio of 0.5 are considered. Results of the experimental investigation are compared, in the subsonic Mach number range, with those obtained by use of a theoretical analysis based on a numerical solution of the integral equation of subsonic lifting-surface theory. A total of 30 dynamic-pressure gages were located at 5 spanwise stations within a wing mounted on a mechanism which forced the wing to undergo a pitching oscillation at the resonant frequency of the system.

Data were obtained for the wing oscillating $\pm 1.5^{\circ}$ about mean angles of attack of 0°, 5°, and 10° over a Mach number range from 0.40 to 1.07, a reduced-frequency range from 0.058 to 0.269, and a Reynolds number range from 6.0×10^6 to 10.2×10^6.

Comparisons with theory of the measured aerodynamic force, moment, and pressure coefficients and respective phase angles, when the wing was at a mean angle of attack of 0°, showed generally good agreement. At 5° and 10° mean angles of attack, the experimental data indicate variations probably caused by shock waves and flow separation.

INTRODUCTION

A need exists for experimental measurements of oscillating air forces because of their importance in flutter and related fields and in order to assess current theoretical work. Despite the importance of the problem, only limited experimental data exist for restricted ranges of

aspect ratio, Mach number, and Reynolds number. Reference 1 includes an extensive bibliography and discusses the present position of the measurement of oscillatory derivatives as well as various methods employed to determine unsteady air loads. In addition, there are, of course, analytical procedures available for the determination of unsteady aerodynamic forces and moments. With the aid of advances in high-speed computing equipment, procedures have been developed for obtaining the aerodynamic forces associated with the particular planform of interest with its specific modes of oscillation. One such procedure, commonly referred to as the kernel function procedure, has been employed in the present investigation. This procedure, which involves a numerical solution of the integral equation of subsonic lifting-surface theory, is described in references 2 and 3. The present investigation was undertaken with the aim of correlating analytically and experimentally determined aerodynamic forces, moments, and pressure distributions.

L 1 6 6 8

Presented in this paper are the force, moment, and pressure coefficients associated with the pitching oscillations about the root midchord of a half-span wing having an aspect ratio of 3 and a taper ratio of 0.5. These experimentally determined coefficients were measured over a reduced-frequency range from 0.058 to 0.269 and a Mach number range from 0.40 to 1.07. The Reynolds number, based on average chord, varied from 6.0×10^6 to 10.2×10^6. The measurements were made by using a forced resonant oscillation technique in the Langley 16-foot transonic tunnel on a wing equipped with a total of 30 miniature electrical pressure gages located at 5 spanwise stations. The chordwise distribution of oscillating pressure coefficients and the spanwise distribution of section forces and pitching moments together with their respective phase angles are compared with the results of calculations based on the kernel function procedure in the subsonic Mach number range.

SYMBOLS

A	aspect ratio
$C_{L,\alpha}, C_{M,\alpha}, C_{p,\alpha}$	complex total lift, total pitching-moment, and pressure coefficients due to pitching oscillation; for example, for lift, $C_{L,\alpha} = (C_{L,\alpha})_r + i(C_{L,\alpha})_i$
c	wing chord at station, ft
$c_{l,\alpha}, c_{m,\alpha}$	complex section lift and section pitching-moment coefficients due to pitching oscillation; for example, for section lift, $c_{l,\alpha} = (c_{l,\alpha})_r + i(c_{l,\alpha})_i$

c_o reference chord (root chord of wing), ft

$i = \sqrt{-1}$

k reduced-frequency parameter, $\frac{c\omega}{2V}$

L_α total lift, positive upward, $|\alpha| qSC_{L,\alpha}$, lb

l_α section lift, $|\alpha| qcc_{l,\alpha}$, lb/ft

M Mach number

M_α total pitching moment about pitch axis, positive with leading edge up, $|\alpha| qSc_oC_{M,\alpha}$, ft-lb

m_α section pitching moment about pitch axis, $|\alpha| qc^2c_{m,\alpha}$, ft-lb/ft

Δp complex pressure difference, lower-surface pressure minus upper-surface pressure, $q|\alpha|C_{p,\alpha}$, lb/sq ft

q dynamic pressure, lb/sq ft

R Reynolds number

S area of wing, sq ft

V velocity of airstream, ft/sec

α angle of attack, positive when leading edge is up, deg

α_m mean angle of attack, static condition, deg

$\phi_{L,\alpha}, \phi_{M,\alpha}, \phi_{p,\alpha}$ phase angle between total lift, total pitching moment, and pressure, respectively, and displacement in pitching oscillation (positive phase angle indicates that lift, pitching moment, or pressure difference Δp leads displacement), deg; for example, for phase angle between total lift and angular displacement,

$$\phi_{L,\alpha} = \tan^{-1} \frac{(C_{L,\alpha})_i}{(C_{L,\alpha})_r}$$

$\phi_{l,\alpha}, \phi_{m,\alpha}$ phase angle between section lift and section pitching moment, respectively, and displacement in pitching oscillation, deg; for example,

$$\phi_{l,\alpha} = \tan^{-1} \frac{(c_{l,\alpha})_i}{(c_{l,\alpha})_r}$$

ω circular frequency of oscillation, radians/sec

$| \; |$ absolute value or modulus

Subscripts:

i,r imaginary and real components

EXPERIMENTAL INVESTIGATION

Apparatus

Tunnel.- The tests were made in the Langley 16-foot transonic tunnel which is a conventional slotted-throat tunnel operating at atmospheric stagnation pressure. A detailed description of this tunnel is given in reference 4.

For these tests, the wing was mounted on the side wall of the tunnel as shown in figure 1. A temperature and pressure survey made in the test section of the tunnel at the locale of the wing prior to conducting the test program indicated that satisfactory flow conditions did exist over the wing surface where the pressure gages were installed. The boundary layer dissipated between 0.089 semispan and 0.178 semispan; this dissipation indicated that the inboard, or 0.17 semispan, pressure gages were essentially unaffected by tunnel boundary conditions. The airstream Mach number profile across the wing span was uniform outside the boundary layer but a temperature and accompanying velocity gradient existed for which a calibration was made and used in the data reduction.

Wing model.- The 45-inch-semispan unswept wing model had a tapered planform with a 40-inch root chord and a 20-inch tip chord. The wing was of thick-skin steel construction and had an NACA 65A005 airfoil section. It contained 6 rib sections with the 30 dynamic-pressure gages located as indicated in figures 2 and 3. Figure 3 is a photograph of the mechanism and model with the wing upper surface removed. Miniature pressure gages were installed in the rib sections between the upper and lower wing shells as indicated in figure 4. The wing structure was designed to have high resonant frequencies. With the root of the wing rigidly clamped, the first bending frequency was 87 cps and the first

torsional frequency was 104 cps. However, when the wing was mounted in the oscillating mechanism, the first bending frequency of the wing-support system was 24.5 cps and the first torsional frequency was 12.5 cps.

Oscillating mechanism.- The oscillating mechanism used in this investigation was similar to the one described in reference 5 except that the electromagnetic shaker was replaced by a hydraulic shaker, as shown in figures 3 and 5. The wing model was mounted through the side wall of the tunnel on the oscillating mechanism that may be considered essentially a torque rod which is supported by bearings near the wing root and fixed at the far end. The semispan wing was attached to the torque rod through a root clamp whose outer edge was flush with the tunnel wall. In order to increase the bending natural frequency of the wing—torque-rod assembly, the stiffness was increased in the vertical bending direction by webs welded to the top and bottom of the torque rod, which can be seen in figures 3 and 5.

The hydraulic system (figs. 3 and 5), which furnished torque to the mechanism, consisted of two small hydraulically operated pistons, servovalves, oil filters, an oscillator, and a hydraulic pump.

A fairing was placed over, and moved with, the root of the wing (fig. 1) to provide smooth airflow. The wing was forced to oscillate $\pm 1.5^{\circ}$ in pitch about the 50-percent-root-chord point at the natural frequency of the wing—torque-rod system by applying a harmonically oscillating torque through the hydraulic shakers attached to the torque rod. The wing was placed successively at mean angles of attack of 0°, 5°, and 10°.

Instrumentation and Calibration

Instrumentation.- The instrumentation provided signals that were a measure of the section lifts, section moments, and pressures on the wing and the angular displacement of the wing at any instant. A block diagram of the instrumentation is shown in figure 6.

There were 30 miniature electrical pressure gages whose locations, both chordwise and spanwise (indicated on fig. 2), were determined on the basis of a desired Gaussian numerical integration scheme, as described in reference 6, in order to obtain the maximum accuracy of integrated lift and moment for the number of gages used. These gages measured the pressure differences between the upper and the lower surfaces of the wing and are described in reference 7. The first two gages in each chordwise row had a ±15-psi range and all the other gages had a ±8-psi range. All the gages and associated recording instrumentation had a flat frequency response to frequencies well above those at which the wing was oscillated during the tests. The electrical impulses from the pressure gages were

fed both to an integrator, which was weighted according to the Gaussian numerical integration scheme so as to measure first the section lift and then, by switching, the section moment, and to a carrier amplifier system to measure the individual pressures. The electrical signals representing both the integrated pressures and the individual pressures were recorded on oscillographs and the electrical signals proportional to the integrated pressures representing either the section lift or the section moment were switched into a resolver system to be recorded on the automatic readout instrument.

The resolver system consisted of a precision motor that drives seven resolvers on the same shaft. The output of the first resolver controlled the hydraulic actuators for forcing the wing oscillations. The second resolver was used as the reference to obtain the in-phase and out-of-phase components of the angular position of the wing. The remaining five resolvers were used to measure signals that were proportional to the in-phase and out-of-phase components of the section lift and the section moment relative to the angular displacement at the five spanwise stations. A discussion of the basic resolver system of measuring complex air forces is found in the appendix of reference 8.

The signal representing the angular position of the root of the wing was obtained from a strain-gage bridge located on the torque rod of the oscillating mechanism. The angular-position signal was fed through a carrier amplifier to both the oscillograph recorder and to the resolver system. In order to obtain the local angular displacements and the bending deflections at the location of the pressure gages, a photographic technique was used in which a camera was located behind a slot across the tunnel test section and below the level of the wing to take blur pictures of lines painted on the bottom of the oscillating wing at every test point. The series of painted stripes on the wing can be seen in figure 1. The camera was set at an angle of 11° below the plane of the wing when $\alpha_m = 0°$.

Calibration.- The pressure gages were individually calibrated by placing a manifold on the upper surface of the wing over the gages and applying various vacuum pressures while the signal variation was recorded. The integrators were adjusted for each semispan station by using a manifold over all the gages in that semispan station for the lift and over the front and rear halves of the station separately for the pitching moment about the midchord. Then the section lift and section moment were calibrated into the oscillograph as well as through the resolver system to the automatic readout setup.

A photographic technique similar to that described in reference 5 was used to calibrate dynamically the angular position of the wing. At the same time that the electrical output of the strain gage on the torque rod was directed to the oscillograph and through the resolvers to the

readout, a blur photograph was obtained of the lines of the wing by using the camera mounted across the test section. The angle of oscillation of any station on the wing could then be related to the amplitude of the signal on the oscillograph or on the readout instruments. In order to simplify the data-reduction process and to set the amplitude of oscillation to the same value for each test point, the resolver was adjusted so that the primary output was the in-phase component of the position signal and the out-of-phase component was negligible.

Test Procedure

Data were obtained for 0°, 5°, and 10° mean angles of attack with the model being driven at the resonant frequency of the wing—torque-rod system through an angle of $\pm 1.5^\circ$ over the Mach number range from 0.40 to 1.07. With the wing at a prescribed mean angle of attack, the tunnel speed was adjusted to a required Mach number, the model was oscillated to the desired amplitude, and the data were recorded on the printout cards and oscillographs. This procedure was repeated at other Mach numbers until the entire Mach number range was covered.

Figure 7 indicates that for the test Mach number range from 0.40 to 1.07 the reduced-frequency range was from 0.269 to 0.058. The Reynolds number range was from 6.0×10^6 to 10.2×10^6 based on a wing average chord of 2.5 feet.

DATA REDUCTION

Recordings of the signals representing the resultant pressure difference between the upper and lower wing surfaces from the individual pressure gages were somewhat distorted because of harmonics and resonant frequencies. In order to extract the magnitude and phase angle of the fundamental component, the individual traces of the pressure-gage output were analyzed by using a harmonic analysis. A 12-point Fourier analysis was made for the experimental data at 0° mean angle of attack to obtain the magnitudes and phase angles of the fundamental mode. After the magnitude of the fundamental component of the oscillating pressure was determined by using the appropriate calibration factors, tunnel dynamic pressure, and amplitude of oscillation, the pressure coefficient was calculated.

The electrical outputs of the pressure gages for each wing station were electrically integrated to obtain section lift and moment. The signals representing lift and moment were separated into the real and imaginary components by using resolvers and were recorded on IBM punch cards. When the appropriate calibration factor, dynamic pressure q,

wing chord c, and amplitude of oscillation $|\alpha|$ were combined, the automatic computing equipment printed answers corresponding to the real and imaginary section lift and moment coefficients, as well as their phase angles, based on the root angle of the wing. The section lift coefficient due to pitching oscillation is defined as

$$c_{l,\alpha} = \frac{(l_\alpha)_r}{qc|\alpha|} + i\,\frac{(l_\alpha)_i}{qc|\alpha|}$$

and the section moment coefficient is defined as

$$c_{m,\alpha} = \frac{(m_\alpha)_r}{qc^2|\alpha|} + i\,\frac{(m_\alpha)_i}{qc^2|\alpha|}$$

The magnitude is the square root of the sum of the squares of the real and imaginary components and the tangent of the phase angle is equal to the ratio of the imaginary component to the real component; that is,

$$\left|c_{l,\alpha}\right| = \sqrt{(c_{l,\alpha})_r^{\,2} + (c_{l,\alpha})_i^{\,2}}$$

$$\phi_{l,\alpha} = \tan^{-1}\frac{(c_{l,\alpha})_i}{(c_{l,\alpha})_r}$$

A positive phase angle indicates that the force leads the displacement in pitching oscillation and is plotted in terms of degrees rather than radians.

As mentioned previously, the wing deformation was determined from studies of photographs showing blurred lines. The amplitude of wing bending of the midchord line is shown as a function of percent semispan for various test Mach numbers in figure 8 for the wing mean angle of attack of 0°. Although the same procedure was used to determine the oscillatory deformations of the wing at $\alpha_m = 5^\circ$ and 10°, the deformations could not be obtained consistently. Since the deformation trends were similar to those for the wing at 0° mean angle of attack, it is believed that the magnitudes of the oscillatory deformations at 5° and 10° mean angles of attack were the same as those at 0° mean angle of attack.

The overall, or total, coefficients were obtained by summing the section forces and moments with appropriate numerical integration factors and then by dividing by the dynamic pressure q, root angle of attack $|\alpha|$, and the total area of the wing S; thus,

$$C_{L,\alpha} = \left(C_{L,\alpha}\right)_r + i\left(C_{L,\alpha}\right)_i = \left(\frac{L_\alpha}{qS|\alpha|}\right)_r + i\left(\frac{L_\alpha}{qS|\alpha|}\right)_i$$

$$C_{M,\alpha} = \left(C_{M,\alpha}\right)_r + i\left(C_{M,\alpha}\right)_i = \left(\frac{M_\alpha}{qSc_o|\alpha|}\right)_r + i\left(\frac{M_\alpha}{qSc_o|\alpha|}\right)_i$$

L
1
6
6
8

and the phase angles were again determined as

$$\phi_{L,\alpha} = \tan^{-1}\frac{\left(C_{L,\alpha}\right)_i}{\left(C_{L,\alpha}\right)_r}$$

$$\phi_{M,\alpha} = \tan^{-1}\frac{\left(C_{M,\alpha}\right)_i}{\left(C_{M,\alpha}\right)_r}$$

ANALYTICAL PROCEDURE

Aerodynamic force, moment, and pressure coefficients for a finite wing oscillating in a deformed pitching mode have been obtained by the kernel function approach described in reference 3. The kernel function procedure is used to calculate the pressure distribution associated with a known distribution of downwash at the wing surface. The downwash on the wing is satisfied at a number of control points and, for this investigation, was determined from the deformed pitching mode of oscillation. Nine control points were used in the calculations and were located at 25, 50, and 75 percent chord for the 20-, 50-, and 80-percent-semispan stations. Once the pressure distribution was known, integrated quantities, such as section or total forces and moments, could be obtained.

RESULTS AND DISCUSSION

The results of this investigation are given in figures 9 to 15. The results are presented in three main groups: pressure coefficients and phase angles, section force and moment coefficients and phase angles, and total or overall coefficients and phase angles as functions of chordwise and spanwise station location and Mach number. Results of a theoretical analysis based on the kernel function procedure are presented for comparison with the experimental data in the subsonic region. At Mach numbers above 0.9, no theoretical values were obtained.

Pressure Coefficients and Phase Angles

The experimental and theoretical pressure distribution for Mach numbers from 0.40 to 1.05 are shown in figures 9 to 11 where pressure coefficients and phase angles are plotted as a function of location in percent chord and percent semispan. The semispan and chord locations for each set of pressure gages are shown in the figures. Experimental data are indicated as open symbols and the results of the analysis are shown as the solid curve on these and all succeeding figures.

The chordwise distribution of pressure coefficients and their respective phase angles are shown for various span locations in figure 9 for $\alpha_m = 0^\circ$ at Mach numbers of 0.40, 0.60, 0.80, 0.90, 0.95, and 1.05. The overall trends of theory and experiment, for both the coefficients and phase angles, agree at all Mach numbers for which theoretical data are presented. The magnitudes of the pressure coefficients are in good agreement at the lower Mach numbers up to $M = 0.80$ (figs. 9(a) and 9(c)) and show some deviation at higher Mach numbers (figs. 9(e) and 9(g)). The deviations probably were caused by oscillatory shock waves and flow separation on the surface of the wing. The experimentally measured coefficients at the higher Mach numbers (figs. 9(i) and 9(k)) are somewhat erratic as might be expected. No clear definition of shock-wave location can be made as is frequently made from steady-state pressure measurements.

The phase angles by which the pressure differences lead or lag the angular displacements are also shown in figure 9. A negative phase angle indicates that the pressure difference lags the angular displacement. Although the results of the experiment and the theoretical analysis agree in trend, the magnitudes of the experimentally determined phase angles differ somewhat from the theoretically determined values. Throughout the Mach number range, the experimentally measured phase angle lags more near the leading edge and leads somewhat more near the trailing edge than theory predicts. At a Mach number of 0.95 (fig. 9(j)) the phase angle changes little over the forward 50 percent of the wing chord but increases

rapidly thereafter. At M = 1.05 (fig. 9(l)) the phase angle increases only slightly over the entire chord at all stations shown with no large increase at the trailing edge. The oscillating pressure exerts a dynamically stabilizing moment about the pitch axis when the phase angle is negative (lagging the displacement) ahead of the pitch axis, or is positive (leading the displacement) in back of the pitch axis. In all other conditions, the pressure exerts a dynamically destabilizing moment. Figure 10 is presented to indicate the unstable regions on the surface of the wing, as determined analytically and experimentally. The results of the analysis predict that the pressure coefficient will be unstable over the surface of the wing between approximately the 15-percent-chord and the 50-percent-chord line throughout the Mach number range. The experimental results indicate an unstable region near the 50-percent-chord line at Mach numbers up to 0.90 with the unstable region moving to the rear half of the wing at Mach numbers of 0.95 and 1.05.

L 1668

The pressure coefficients have been cross plotted to show spanwise distributions in figure 11. In general, both the experimental and theoretical pressure coefficients decrease as the wing tip is approached. It may be concluded that for pitch oscillation about $\alpha_m = 0^\circ$ good agreement between experiment and theory has been obtained for the oscillatory pressure coefficients up to a Mach number of 0.80, although the theory does not account for shock waves at transonic speeds.

Section Lift and Moment Coefficients and Phase Angles

Section pitching-moment coefficients.- The section pitching-moment coefficients and their respective phase angles are given in figure 12 for mean angles of attack of 0°, 5°, and 10°. The root angular oscillation was $\pm 1.5^\circ$ at all mean angles of attack. For reference, theoretical data are plotted in figure 12 for all three mean angles of attack even though theory might not be applicable to the higher angles.

The agreement between theoretically and experimentally determined section moment coefficients is very good for 0° mean angle of attack (fig. 12(a)). The experimental data are sufficiently consistent to indicate no radical deviation near a Mach number of 1.00. The moment data for the higher mean angles of attack (figs. 12(c) and 12(e)) also indicate that the coefficients are consistent above M = 0.95 with the exception of the coefficients at the 62-percent-semispan station for a mean angle of attack of 10°.

At wing mean angles of attack of 5° and 10° (figs. 12(c) and 12(e)), some deviation between experimental values and theoretical values occurs as might be expected since the theory does not account for wing mean angle of attack. At high Mach numbers (above 1.00) coefficients for both 5° and 10° mean angles of attack are considerably less than those

for 0° mean angle of attack. The moment coefficients for 10° mean angle of attack are considerably smaller than those for the other mean angles.

Section pitching-moment phase angles.- The phase angles corresponding to the section pitching-moment coefficients for the various mean angles of attack are also shown in figure 12. Very good agreement exists between theory and experiment for $\alpha = 0°$ and 5° through nearly the complete range where theoretical data are presented. At $M = 0.90$, the experimental values tend to decrease more rapidly than the theoretical results. In the transonic speed range, $M = 0.90$ to $M = 1.05$, there is considerable scatter in the data, especially at 5° mean angle of attack (fig. 12(d)). Apparently, the oscillating shock waves on the wing cause the phase angle to move erratically.

At 10° mean angle of attack the phase angles are positive over the three middle pressure-gage stations up to $M = 0.90$ (fig. 12(f)). The positive sign of the moment phase angle indicates a dynamically destabilizing moment - that is, the aerodynamic damping has changed sign and the oscillation no longer has the tendency to damp out or have a decaying oscillation. The negative phase angles of the root and tip stations indicate stabilizing moments. Fortunately, the internal damping of the wing—torque-rod assembly was sufficient to keep the wing configuration stable in the tunnel. Evidence of the stalled condition is indicated in figure 12(f) where the section moment phase angle with the mean angle of attack of the wing at 10° is in the unstable region over most of the wing through a large Mach number range. As a matter of interest, it may be pointed out that, when an attempt was made to obtain data at 15° mean angle of attack, stall flutter was encountered at a Mach number of 0.40.

Section lift coefficients.- The section lift coefficients and their respective phase angles are given in figure 13 for mean angles of attack of 0°, 5°, and 10°. In general, the experimentally and theoretically determined section lift coefficients for the wing at 0° mean angle of attack (fig. 13(a)) follow the same trend with the analytical values higher; that is, the wing felt less oscillatory force than was predicted and, therefore, a calculated flutter speed would probably be lower than the actual flutter speed. The data are consistent in the transonic speed range with the exception of those for the 38-percent-span station.

The section lift coefficients for 5° mean angle of attack are presented in figure 13(c). The experimental and theoretical results are in good agreement for the three inboard spanwise stations, whereas the theoretical values fall below the experimental results for the two outboard spanwise stations. The theory does not consider any mean angles of attack other than 0° and the higher experimental coefficients at the outboard stations may be caused by tip effects and flow separation.

The experimental lift coefficients for 10° mean angle of attack (fig. 13(e)) indicate values higher than those for 0° mean angle of attack at Mach numbers up to 0.70. A similar trend is evident in the data of reference 9. At higher Mach numbers, the values diminish and become less than those for the 0° mean angle of attack. Thus, the effect of increasing wing angle of attack is to increase the lift coefficients in the low Mach number region and to decrease the coefficients in the higher subsonic and low transonic regions.

Section lift phase angles.- The phase angles corresponding to the section lift coefficients also are given in figure 13 for mean angles of attack of 0°, 5°, and 10°. Very good agreement exists between theory and experiment for the 0° mean angle of attack in the Mach number range where theoretical data are presented (fig. 13(b)). Above this range, the phase-angle measurements continue the established trend and become negative at all stations. The same trend is observed for both 5° and 10° mean angles of attack.

L
1
6
6
8

Total Lift and Moment Coefficients and Phase Angles

Total pitching-moment coefficients.- The total pitching-moment coefficients and phase angles are shown in figure 14 for mean angles of attack of 0°, 5°, and 10°. The solid curve represents the theoretical results; the dashed curve represents the theoretical value of the two-dimensional moment coefficient corrected for aspect ratio and compressibility effects by $\frac{A}{A\sqrt{1 - M^2} + 2}$, and the open symbols indicate the experimental data. The theory agrees very well with experiment for 0° mean angle of attack, and the corrected two-dimensional moment coefficient follows a trend similar to that for the moment data but at a larger magnitude. At $M = 0.90$ the experimental coefficients start to decrease as is usually the case for static coefficients. The 10° angle-of-attack data are lower than the 0° and 5° data probably as a result of separated-flow effects.

Total pitching-moment phase angles.- The phase angles corresponding to the overall pitching-moment coefficients are also shown in figure 14. The solid curve represents the results of the theoretical analyses which are in good agreement with the experimental results for $\alpha_m = 0^\circ$ and 5° over the range where theory is presented. The total moment phase angles are little different from the section moment phase angles for 5° and 10° angles of attack, as shown in figure 12. These total moment phase angles for 10° angle of attack are practically all positive as might be expected from the section phase angles (fig. 12(f)). However, a divergent oscillation did not occur since the internal damping was greater than the overall destabilizing aerodynamic damping.

Total lift coefficients.- Theoretical and experimental total lift coefficients and phase angles are shown in figure 15. The results of theory are shown as a solid curve, the two-dimensional lift coefficient corrected for aspect ratio and compressibility effects is indicated by the dashed curves, and the experimental data are indicated by symbols. At a mean angle of attack of 0°, the magnitudes of the experimental and theoretical coefficients show good agreement in trend (fig. 15(a)); but again, as with the section lift coefficients, the theoretical values are moderately greater. Although the lift coefficients obtained from the aspect-ratio correction indicate a similar trend, the magnitudes were considerably higher than the experimental values.

The lift coefficients increase with an increase in mean angle of attack in the lower Mach number range as can be seen at a Mach number of 0.40 and decrease slightly with increasing angle of attack at the higher Mach numbers as indicated at a Mach number of 1.00. The total pitching-moment coefficients followed the same trend in the higher Mach number range (fig. 14(a)).

Total lift phase angles.- The phase angles corresponding to the overall lift coefficients are shown in figure 15(b). Very good agreement occurs between theory and experiment for $\alpha_m = 0^\circ$ in the range of theory shown in the figure. The change of sign of $\phi_{L,\alpha}$ in the transonic Mach number range is encountered for both the section derivatives (fig. 13(b)) and in unpublished data obtained by Leadbetter and Clevenson at the Langley Research Center for a low-aspect-ratio rectangular wing oscillating in pitch at transonic speeds. The phase angles for mean angles of attack of 5° and 10° indicate trends similar to those for $\alpha_m = 0^\circ$. The scatter in the data with the wing at 10° mean angle of attack is caused by flow separation and shock waves on the wing.

CONCLUSIONS

Aerodynamic forces, moments, and pressures, along with their respective phase angles, associated with a deformed pitching oscillation have been measured on an aspect-ratio-3, taper-ratio-0.5 wing by using a resonant oscillation experimental technique. The measurements were made over a range of Mach number from 0.40 to 1.07, a range of reduced frequency from 0.058 to 0.269, and a range of Reynolds number from 6.0×10^6 to 10.2×10^6. In addition, theoretical results, based on experimentally determined mode shapes, have been obtained for comparison in the Mach number range from 0.40 to 0.90. From the results given, the following conclusions are made:

1. The trends of the theoretically and experimentally determined pressure coefficients and phase angles agreed at Mach numbers where theory is presented with the exception of speed ranges where local shock waves and flow separation occur. The magnitudes of the pressure coefficients were in good agreement in the lower Mach number range up to a Mach number of 0.80. The measured coefficients were somewhat erratic in the transonic speed region.

2. The agreement between the theoretically and experimentally determined section moment coefficients and phase angles is very good for 0° mean angle of attack. At higher mean angles of attack, deviations occur in the magnitude of the pitching-moment coefficient; the corresponding phase angle also indicates an unstable condition.

3. The experimentally determined section lift coefficients, although agreeing with theory in trend, indicate that the analysis gives results that are somewhat higher than those measured at 0° angle of attack. At higher angles of attack, the section lift coefficients increased in the low Mach number region and decreased at the higher speeds. The corresponding phase angles are predicted within a few degrees.

Langley Research Center,
National Aeronautics and Space Administration,
Langley Air Force Base, Va., January 25, 1962.

REFERENCES

1. Garrick, I. E.: On the Measurement of Oscillatory Aerodynamic Derivatives Including a Summary of Recent Results. Presented to Structures and Materials Panel of AGARD (Paris, France), May 22-26, 1961.

2. Watkins, Charles E., Runyan, Harry L., and Woolston, Donald S.: On the Kernel Function of the Integral Equation Relating the Lift and Downwash Distributions of Oscillating Finite Wings in Subsonic Flow. NACA Rep. 1234, 1955. (Supersedes NACA TN 3131.)

3. Watkins, Charles E., Woolston, Donald S., and Cunningham, Herbert J.: A Systematic Kernel Function Procedure for Determining Aerodynamic Forces on Oscillating or Steady Finite Wings at Subsonic Speeds. NASA TR R-48, 1959.

4. Ward, Vernon G., Whitcomb, Charles F., and Pearson, Merwin D.: Air-Flow and Power Characteristics of the Langley 16-Foot Transonic Tunnel With Slotted Test Section. NACA RM L52E01, 1952.

5. Widmayer, Edward, Jr., Clevenson, Sherman A., and Leadbetter, Sumner A.: Some Measurements of Aerodynamic Forces and Moments at Subsonic Speeds on a Rectangular Wing of Aspect Ratio 2 Oscillating About the Midchord. NACA TN 4240, 1958. (Supersedes NACA RM L53F19.)

6. Lowan, Arnold N., Davids, Norman, and Levenson, Arthur: Tables of the Zeros of the Legendre Polynomials of Order 1-16 and the Weight Coefficients for Gauss' Mechanical Quadrature Formula. Bull. American Math. Soc., vol. 48, no. 10, Oct. 1942, pp. 739-743.

7. Patterson, John L.: A Miniature Electrical Pressure Gage Utilizing a Stretched Flat Diaphragm. NACA TN 2659, 1952.

8. Queijo, M. J., Fletcher, Herman S., Marple, C. G., and Hughes, F. M.: Preliminary Measurements of the Aerodynamic Yawing Derivatives of a Triangular, a Swept, and an Unswept Wing Performing Pure Yawing Oscillations, With a Description of the Instrumentation Employed. NACA RM L55L14, 1956.

9. Rainey, A. Gerald: Measurement of Aerodynamic Forces for Various Mean Angles of Attack on an Airfoil Oscillating in Pitch and on Two Finite-Span Wings Oscillating in Bending With Emphasis on Damping in the Stall. NACA Rep. 1305, 1957. (Supersedes NACA TN 3643.)

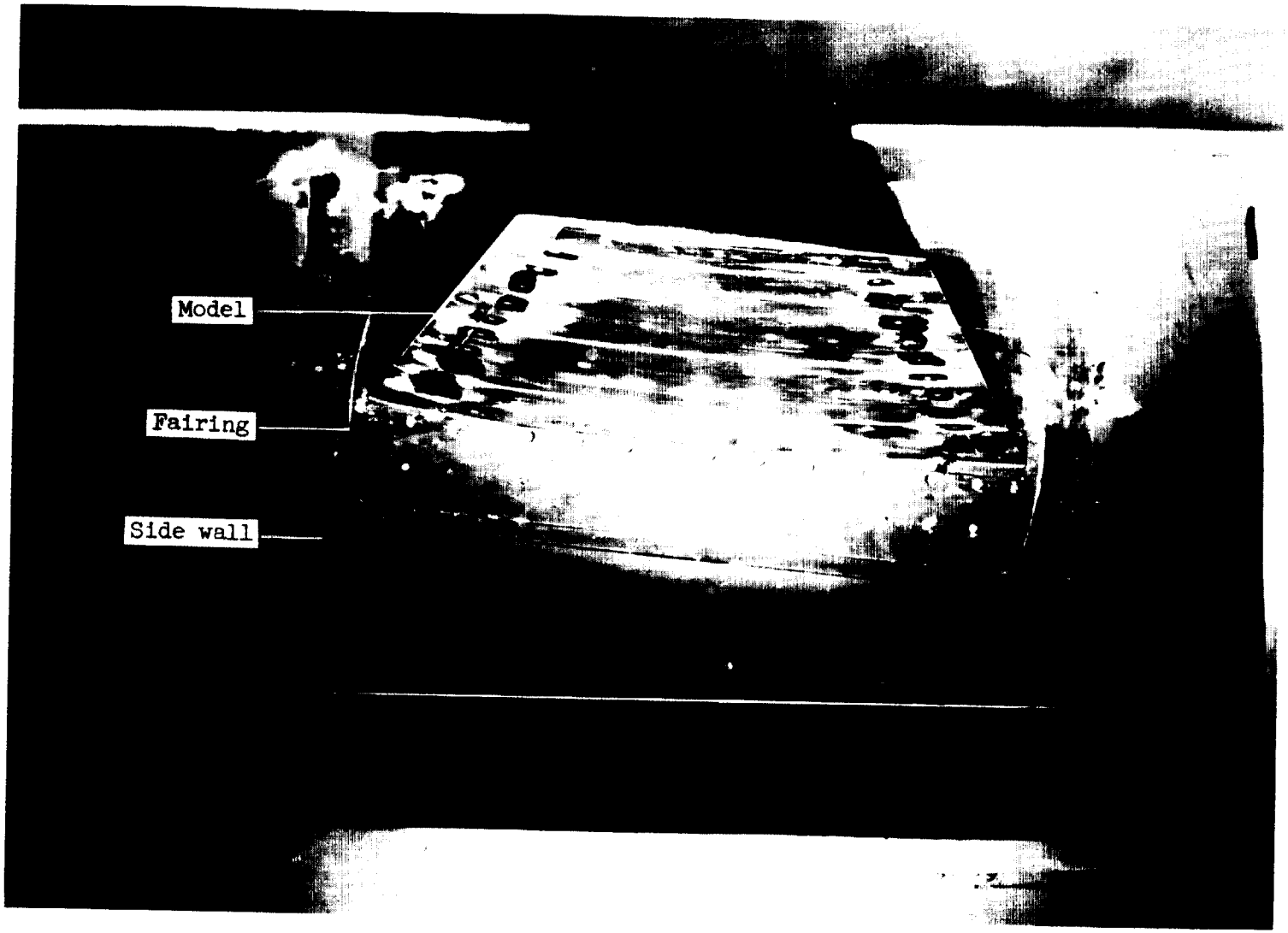

Figure 1.- Model mounted at the side wall of tunnel. $\alpha_m = 5^\circ$. L-62-28

Pressure-Gage Locations							
Percent semispan	Percent chord						
17	2.5	13	30	50	70	87	96
38	2.5	13	30	50	70	87	96
62	3.5	17	38	62	83	95	
83	4.7	23	50	77	94		
97	4.7	23	50	77	93		

+ Pressure gage

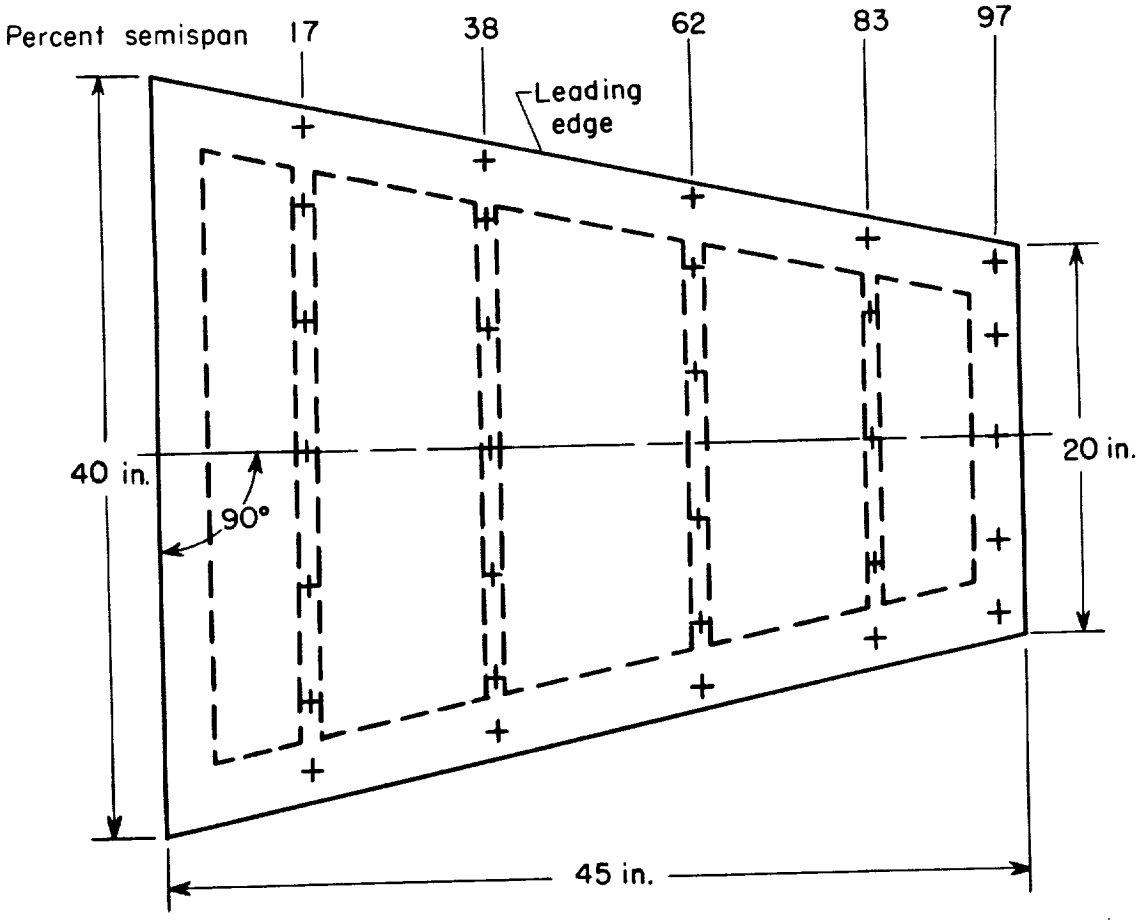

Figure 2.- Schematic diagram of model with pressure-gage locations indicated.

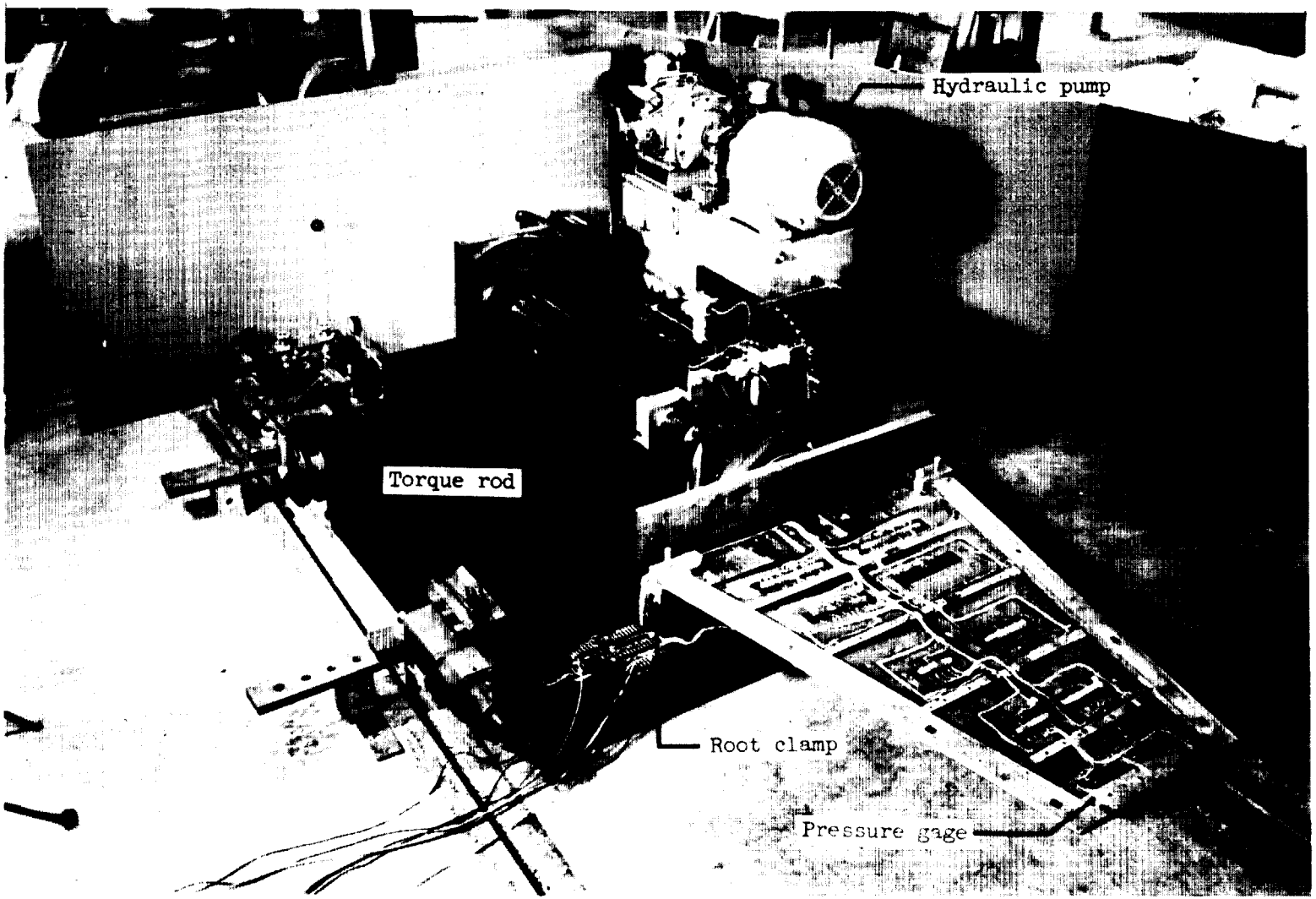

L-58-2195.1

Figure 3.- Oscillating mechanism and model with wing upper surface removed.

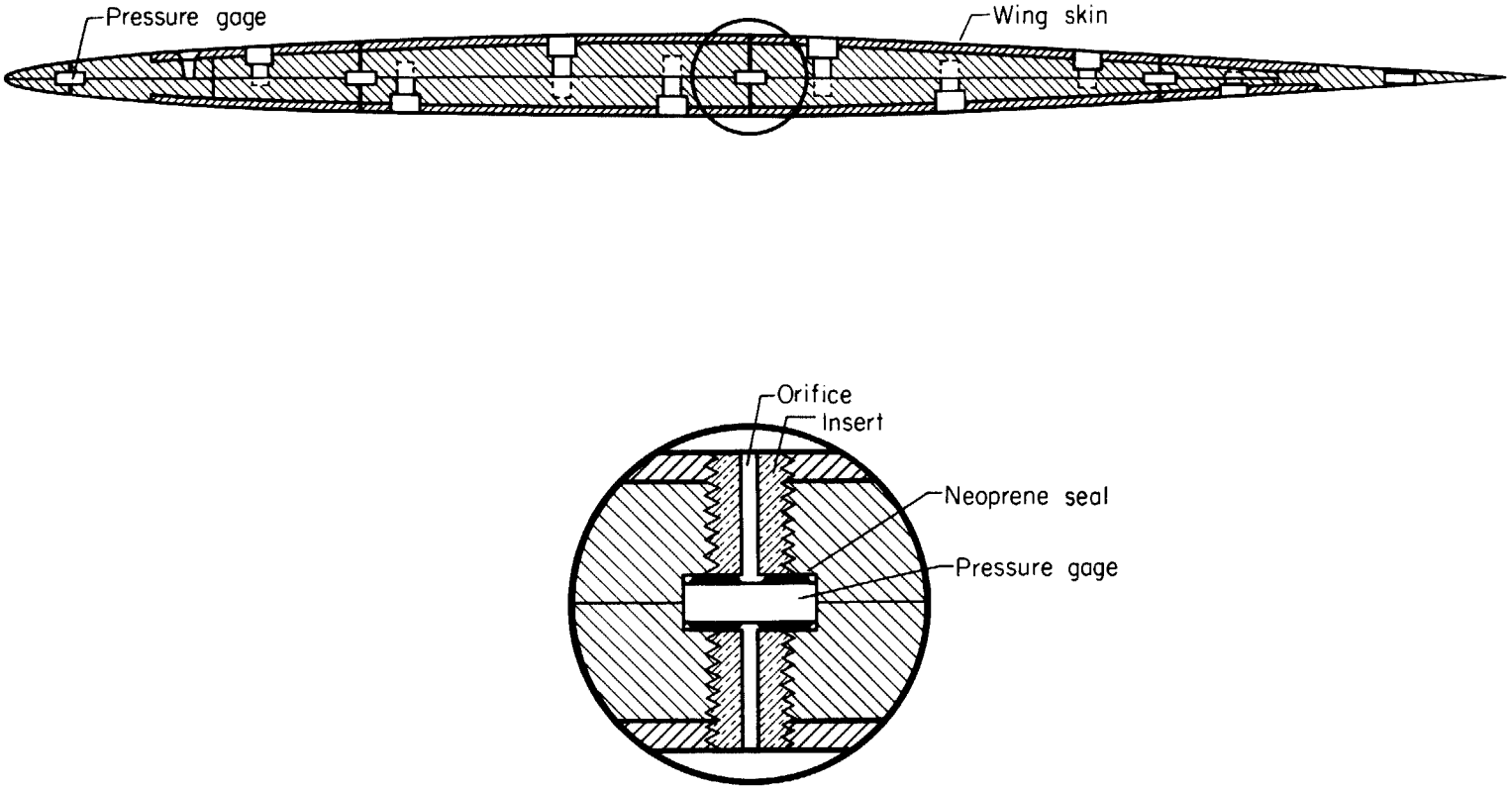

Figure 4.- Sketch of cross section of wing and pressure-gage installation.

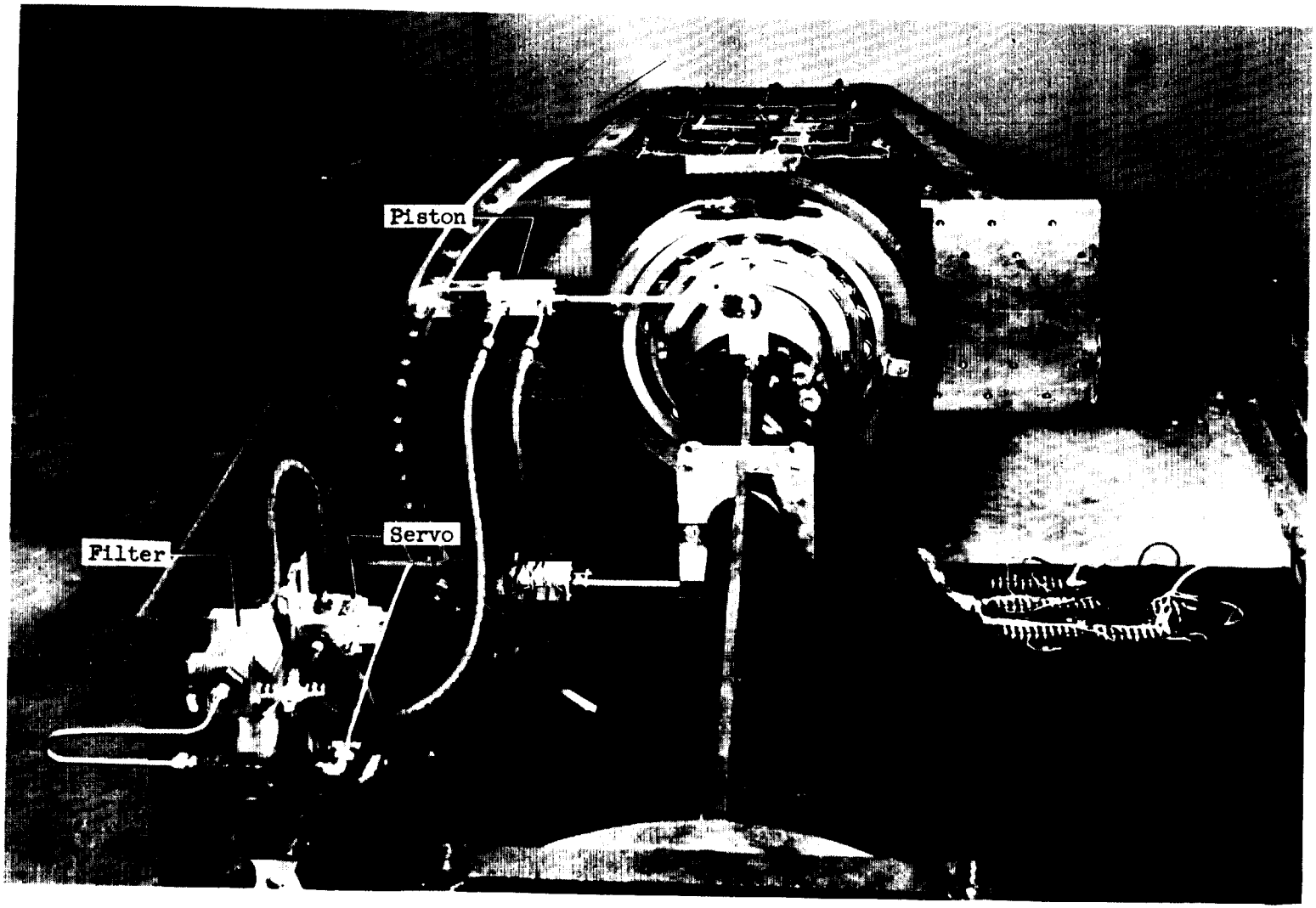

Figure 5.- Oscillating mechanism used in the investigation. L-58-2196.1

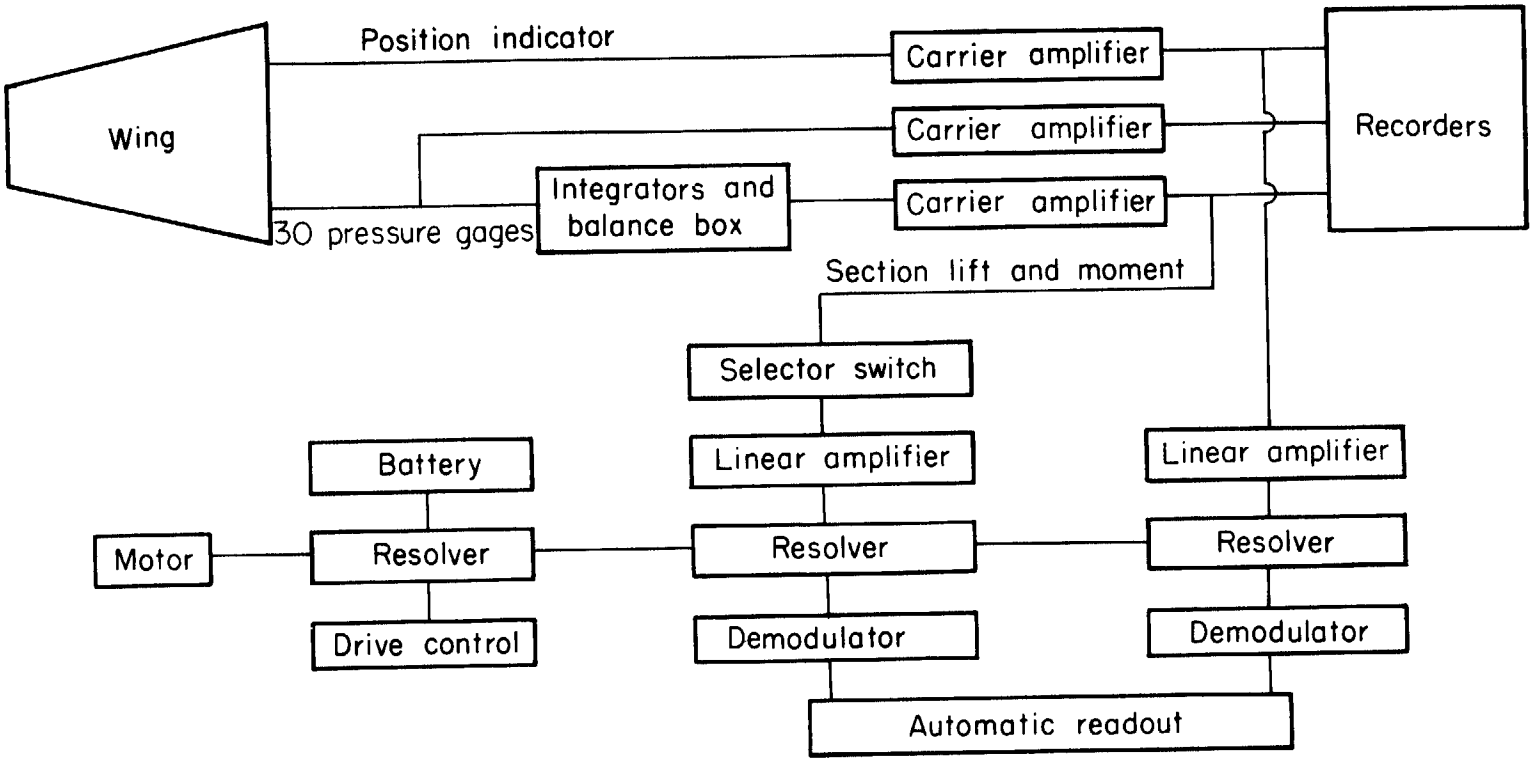

Figure 6.- Block diagram indicating electronic equipment involved in determining oscillatory coefficients.

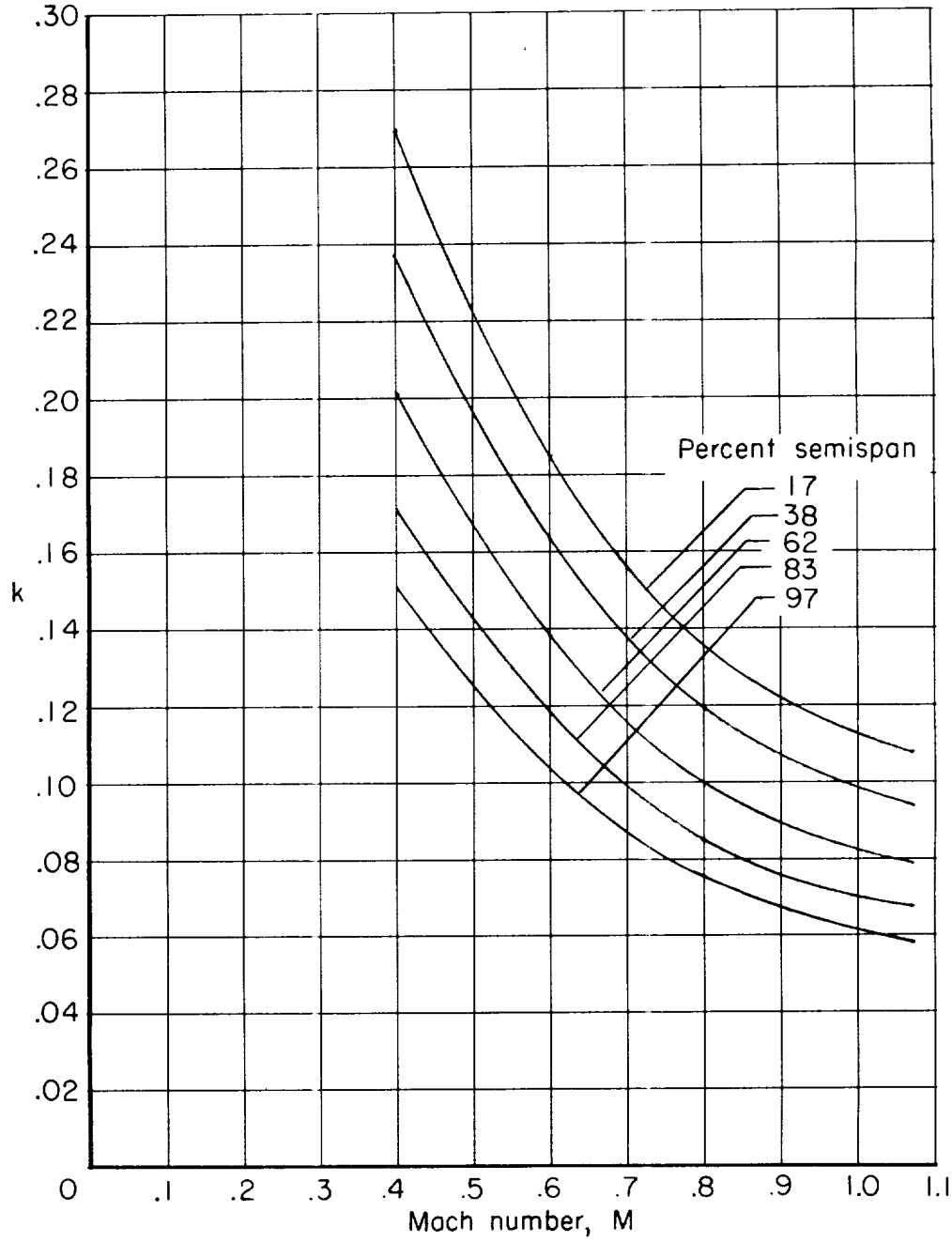

(a) Variation of k with M at several pressure-gage locations.

Figure 7.- Mach number, reduced frequency, and Reynolds number ranges of the experimental investigation.

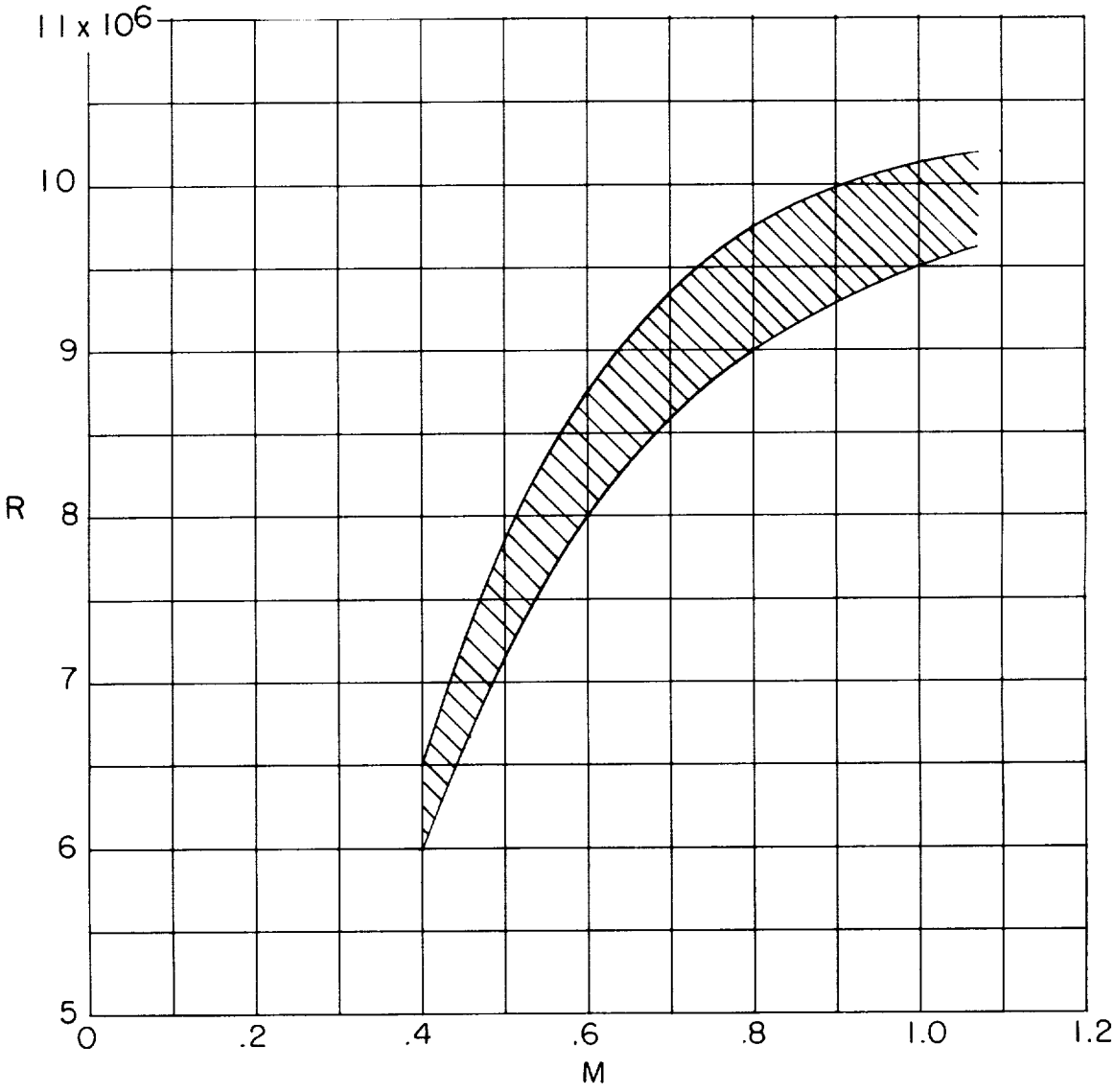

(b) Variation of R with M.

Figure 7.- Concluded.

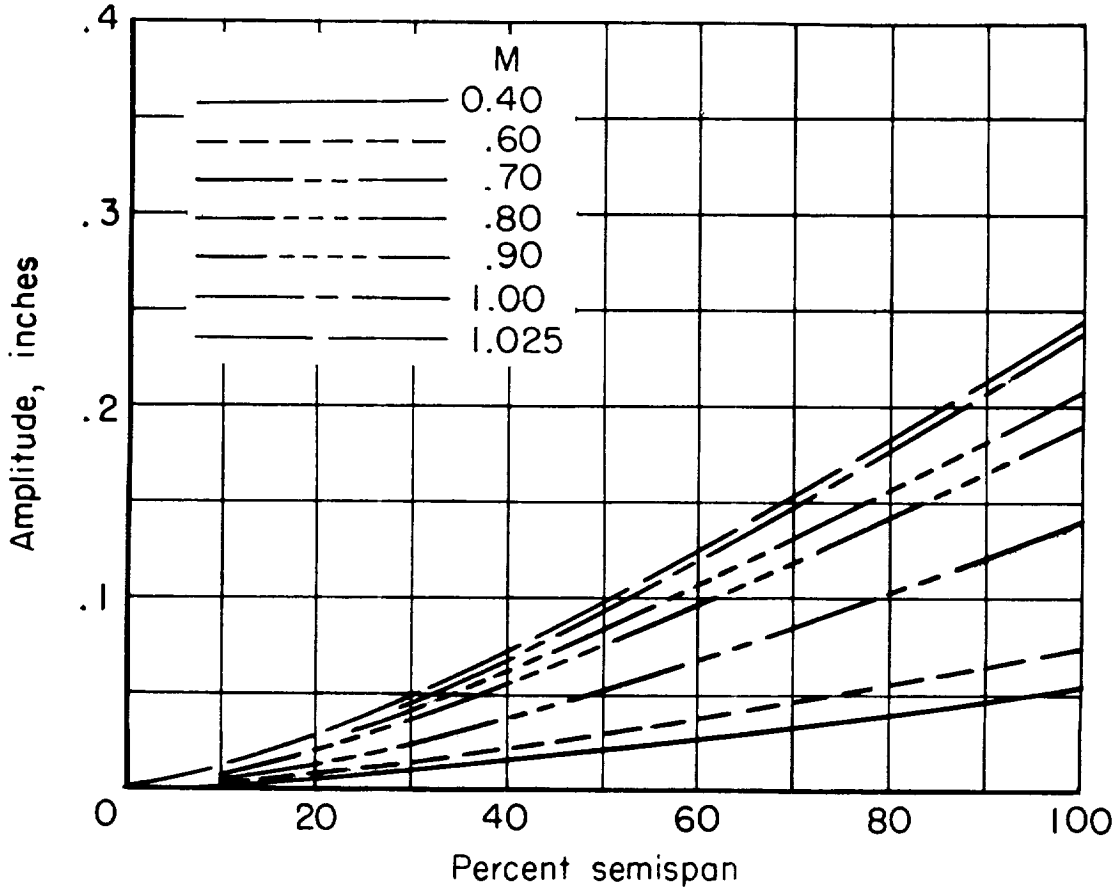

Figure 8.- Amplitude of bending oscillation of the pitch axis as a function of semispan for various Mach numbers.

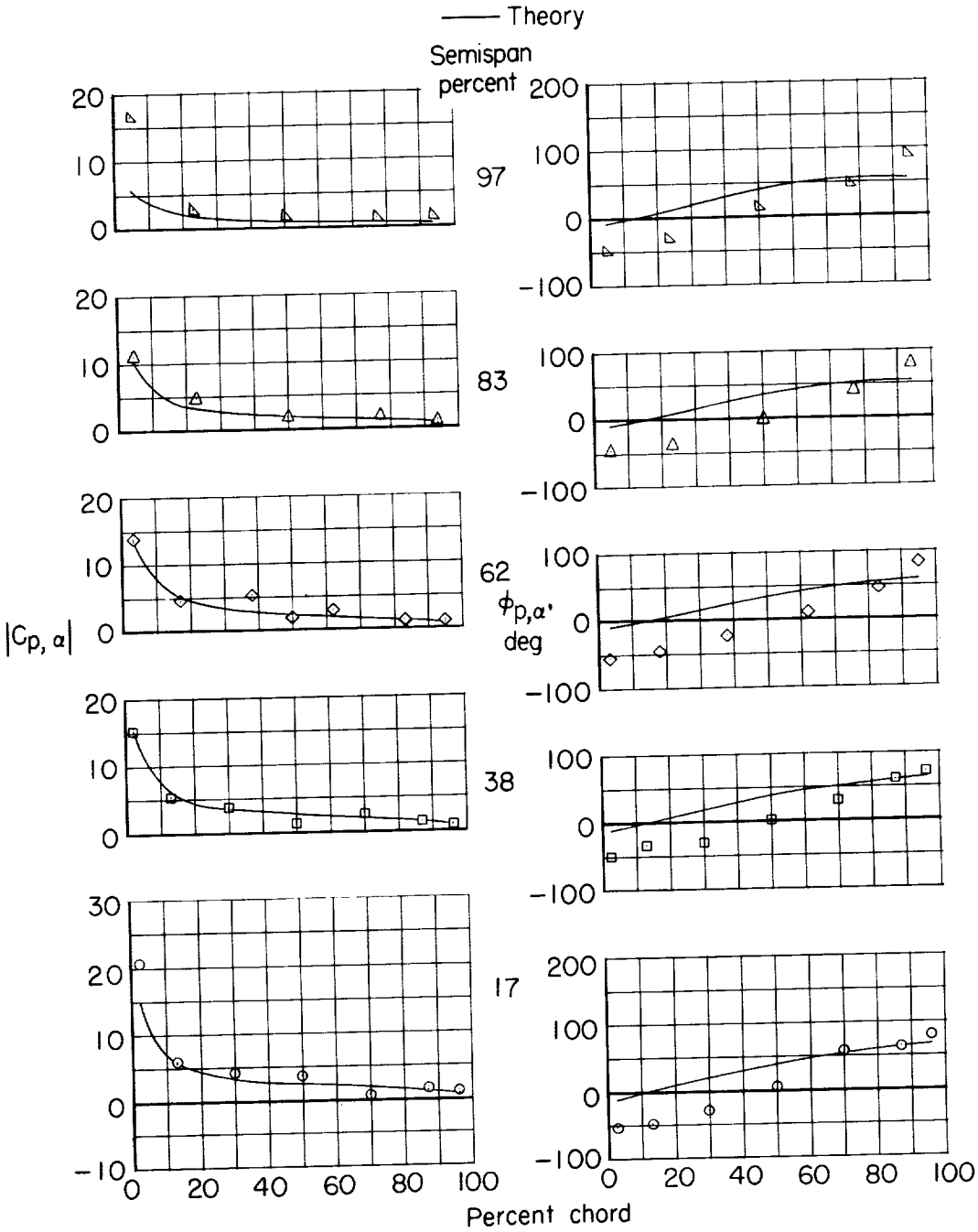

(a) Pressure coefficient for M = 0.40.

(b) Phase angle for M = 0.40.

Figure 9.- Experimental and theoretical chordwise distributions of pressure coefficient and phase angle. $\alpha_m = 0^\circ$.

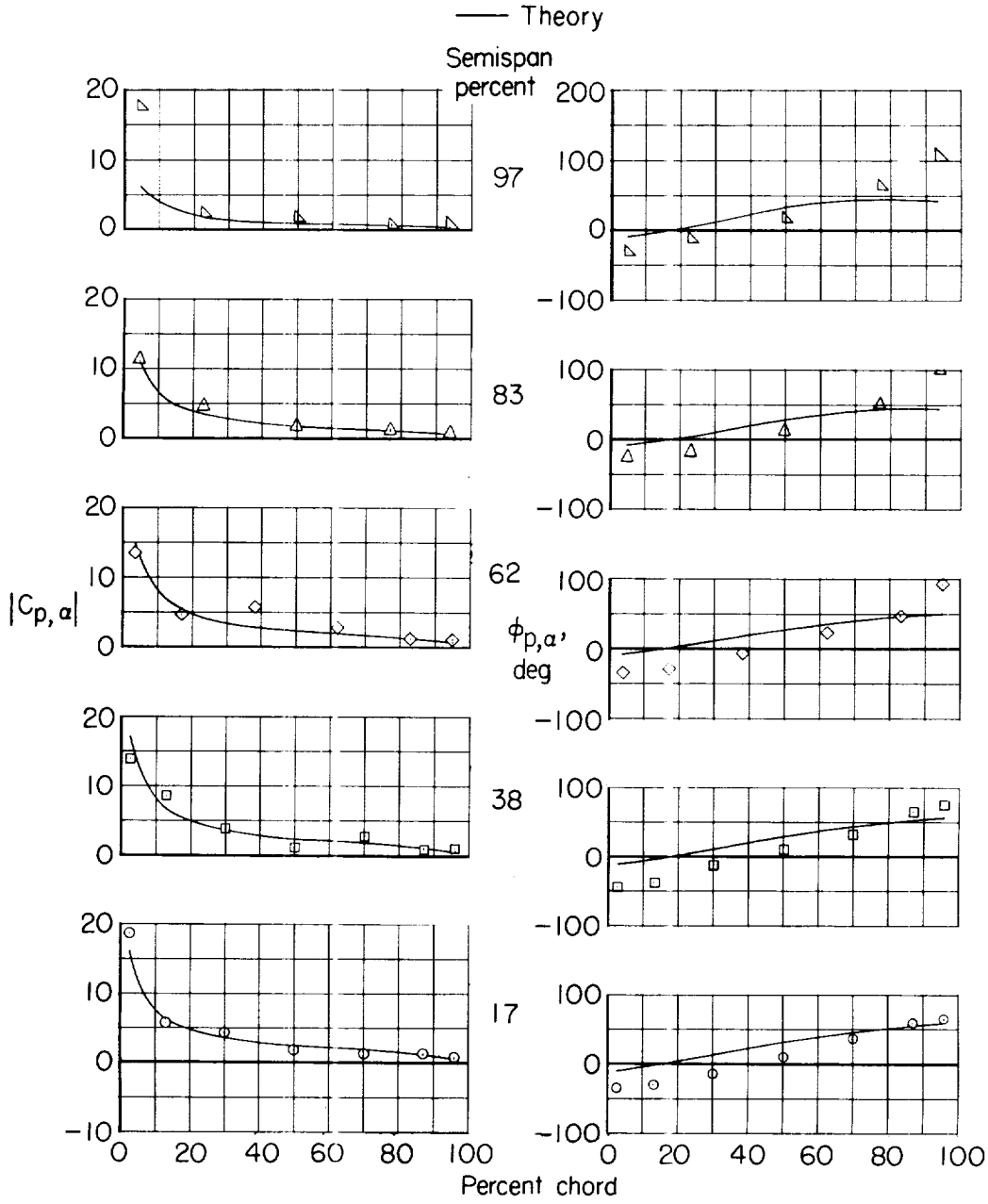

(c) Pressure coefficient for M = 0.60.

(d) Phase angle for M = 0.60.

Figure 9.- Continued.

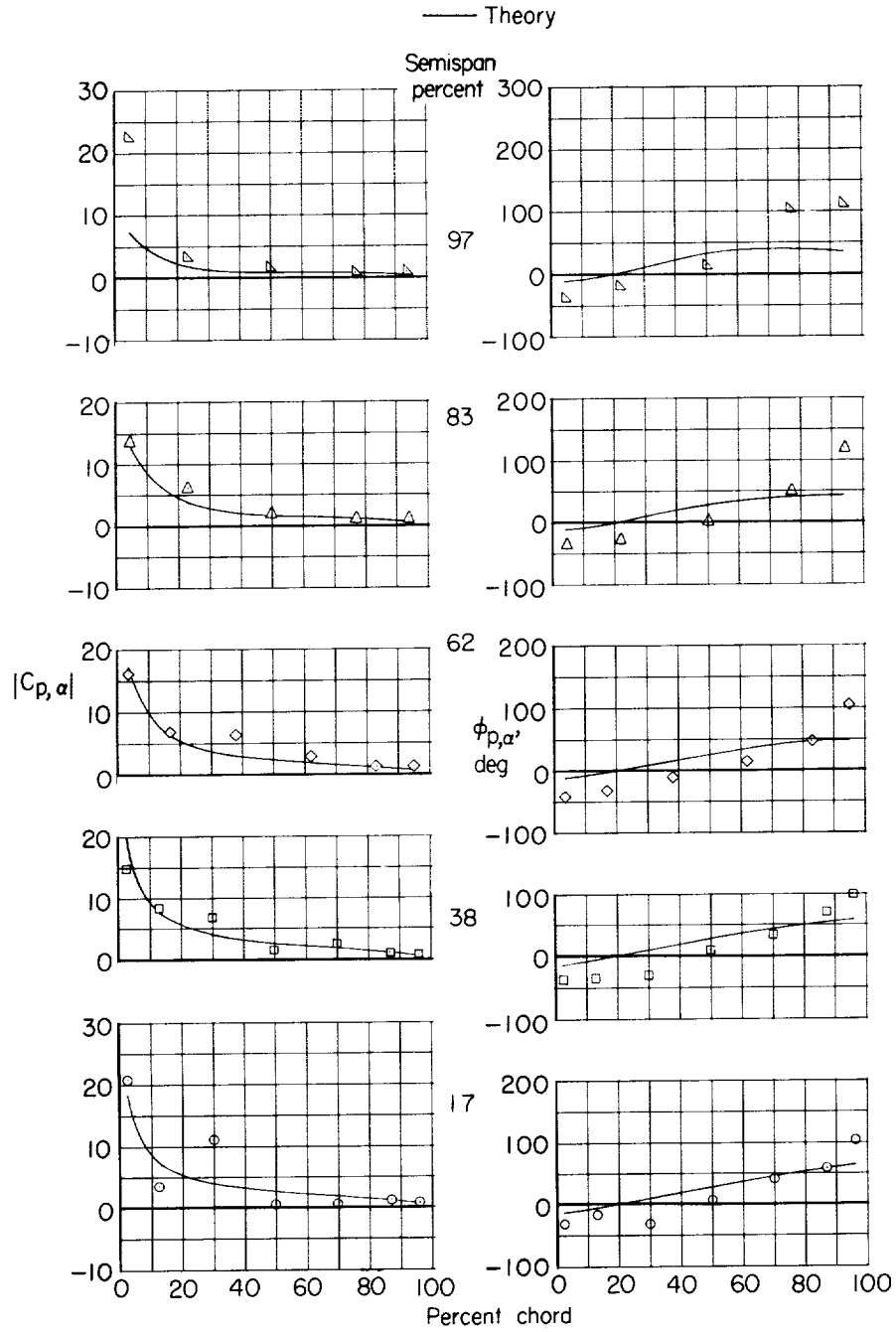

(e) Pressure coefficient for M = 0.80.

(f) Phase angle for M = 0.80.

Figure 9.- Continued.

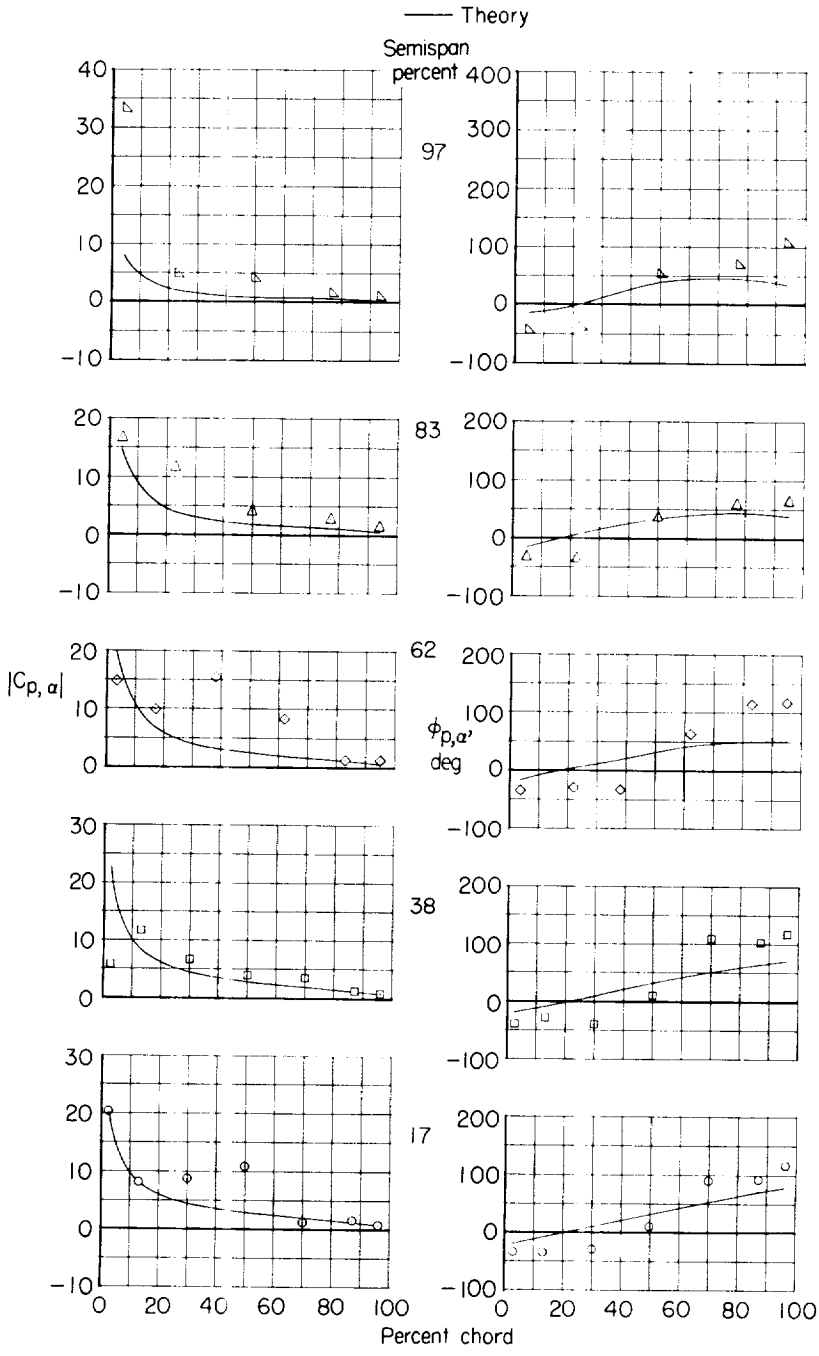

(g) Pressure coefficient for M = 0.90.

(h) Phase angle for M = 0.90.

Figure 9.- Continued.

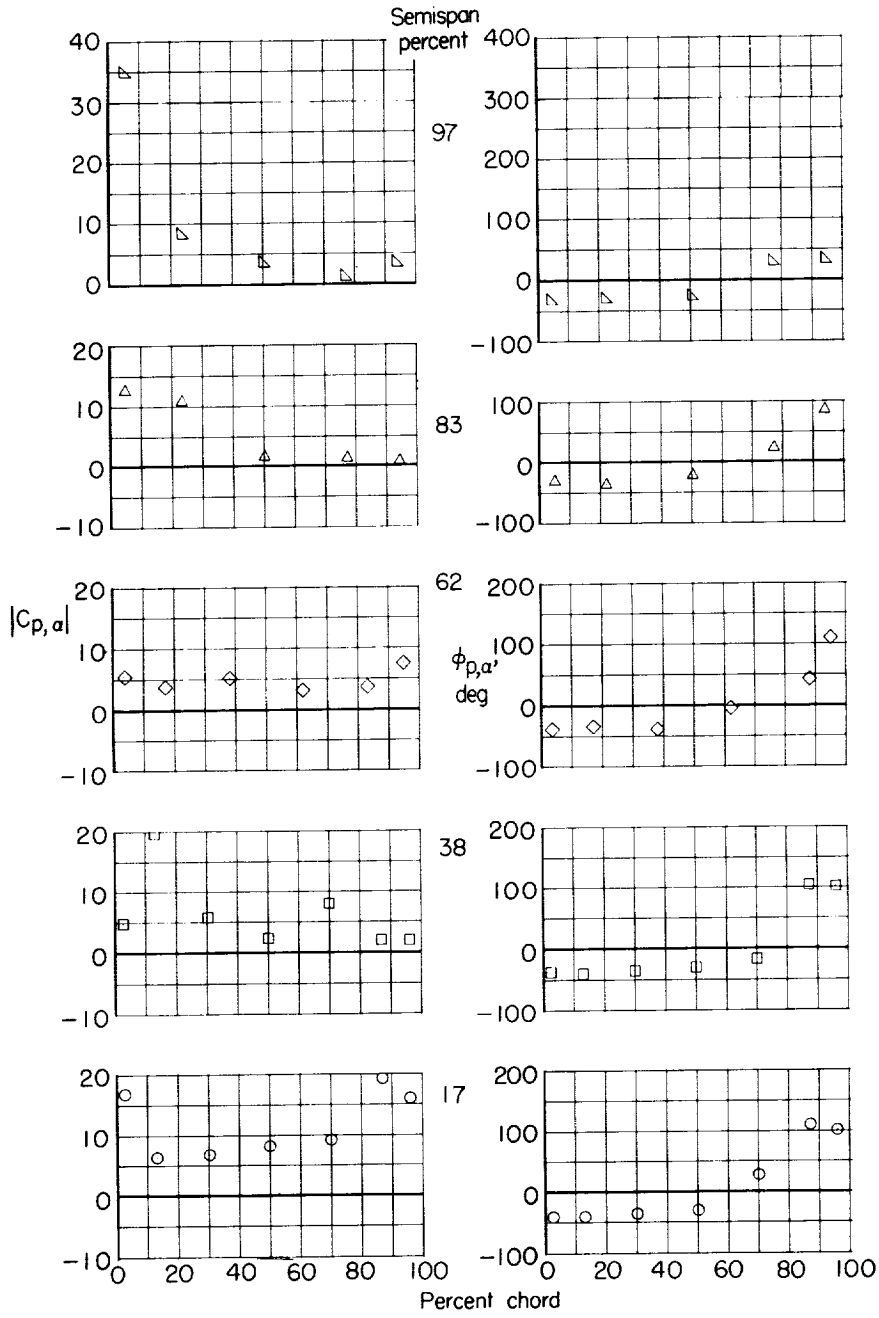

(i) Pressure coefficient for M = 0.95.

(j) Phase angle for M = 0.95.

Figure 9.- Continued.

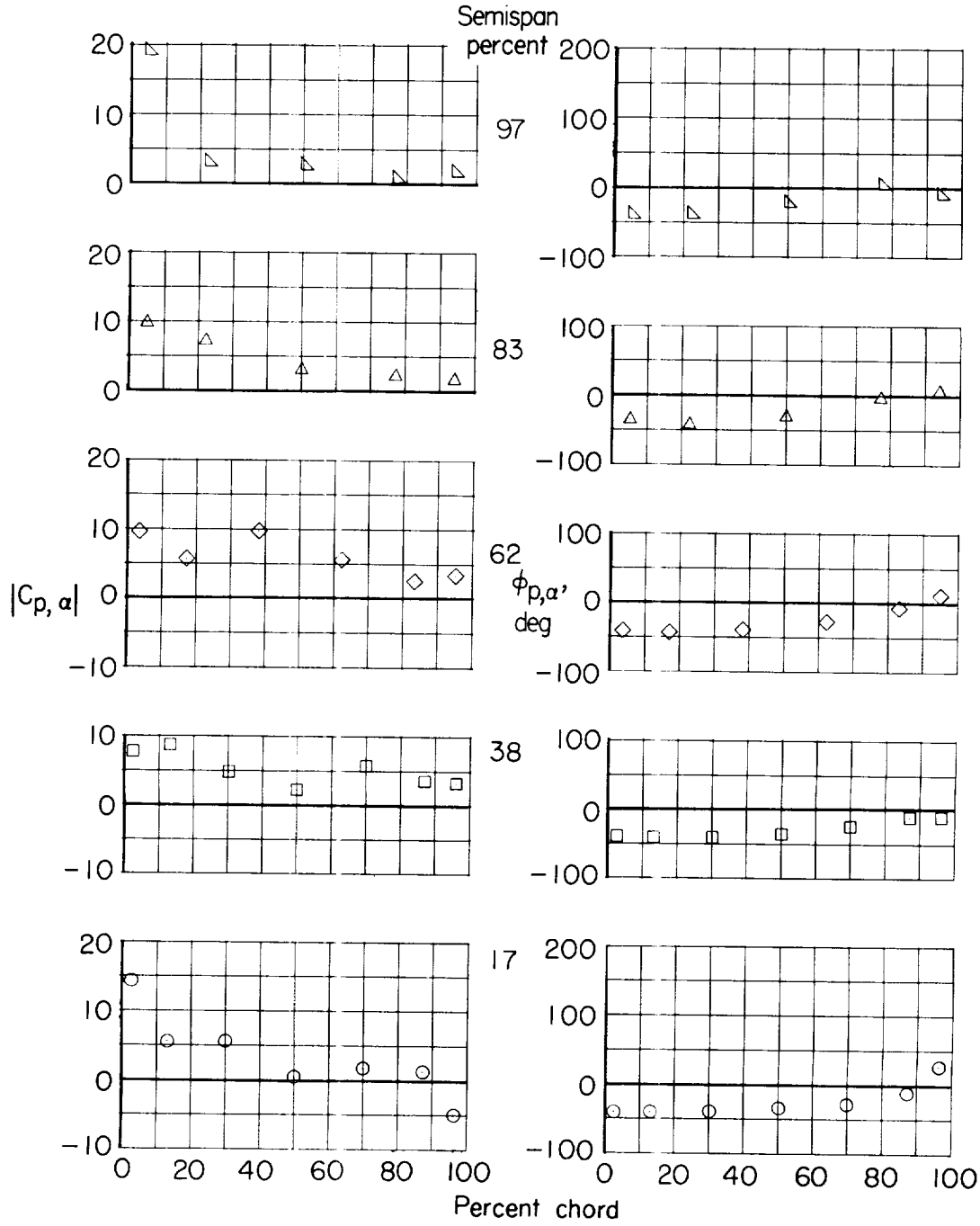

(k) Pressure coefficient for M = 1.05.

(l) Phase angle for M = 1.05.

Figure 9.- Concluded.

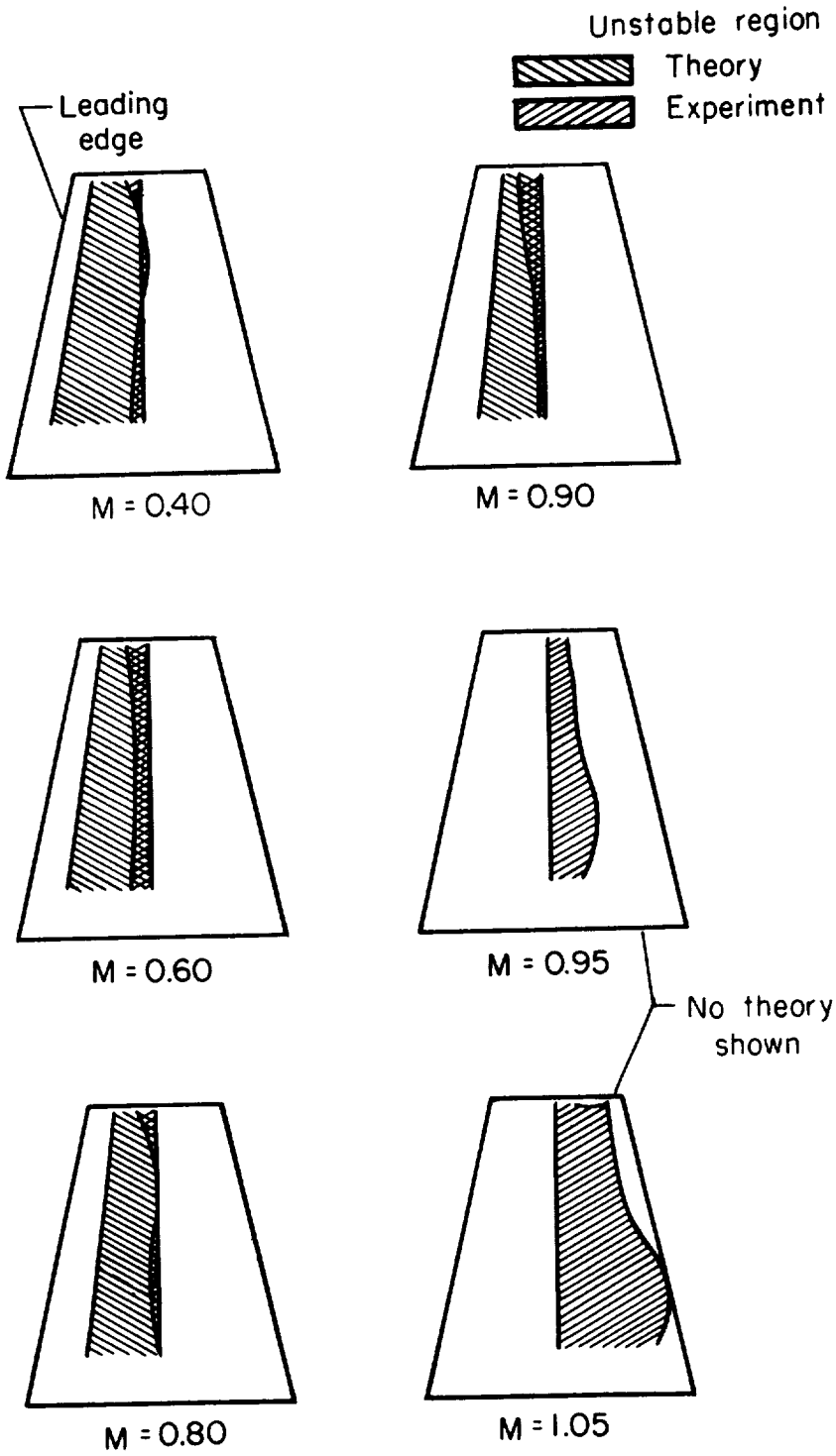

L-1668

Figure 10.- Unstable regions on wing surface as indicated by pressure-coefficient phase angles.

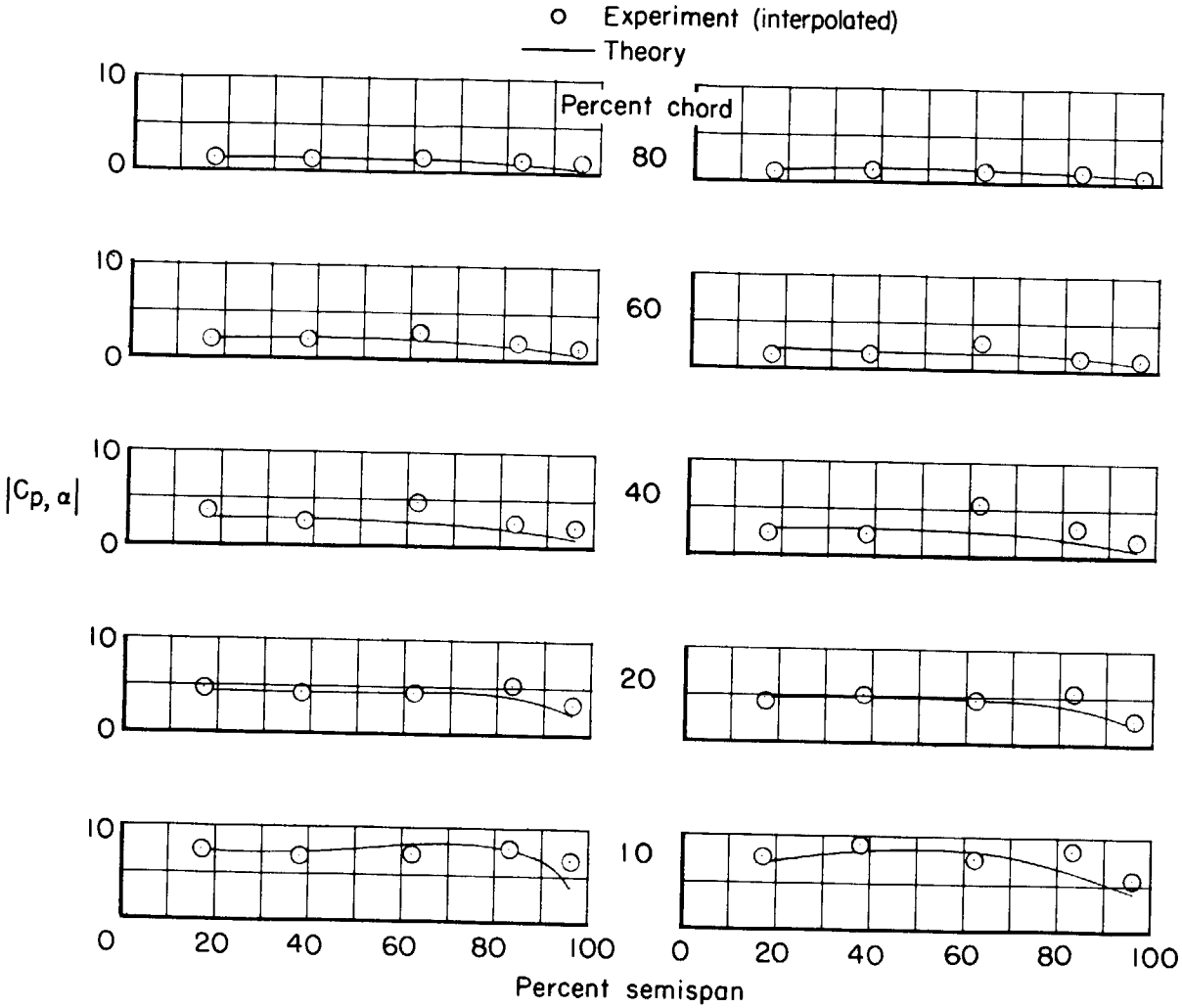

(a) Pressure coefficient for M = 0.40. (b) Pressure coefficient for M = 0.60.

Figure 11.- Cross plots of spanwise distributions of pressure coefficient. $\alpha_m = 0^\circ$.

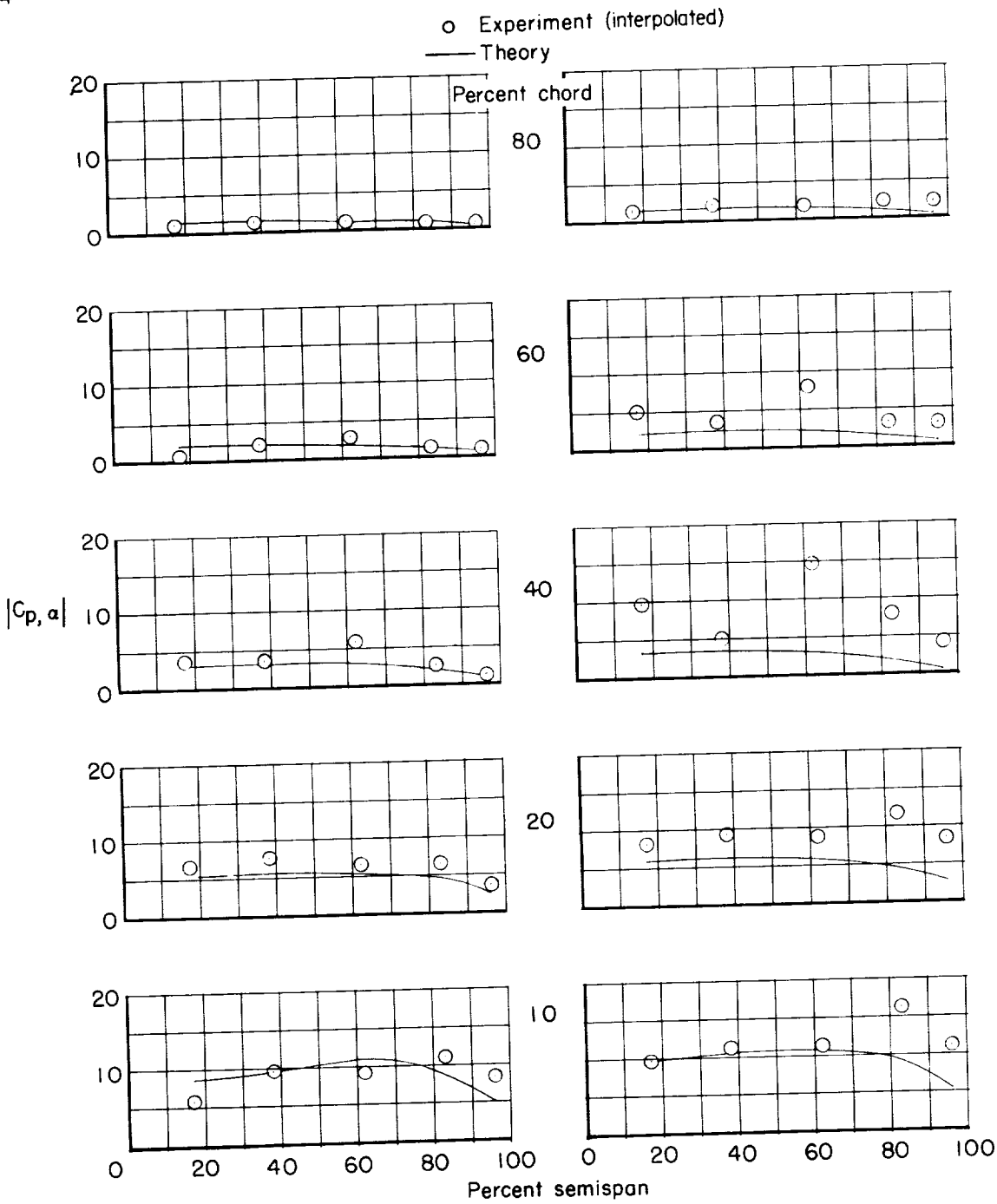

(c) Pressure coefficient for M = 0.80.

(d) Pressure coefficient for M = 0.90.

Figure 11.- Continued.

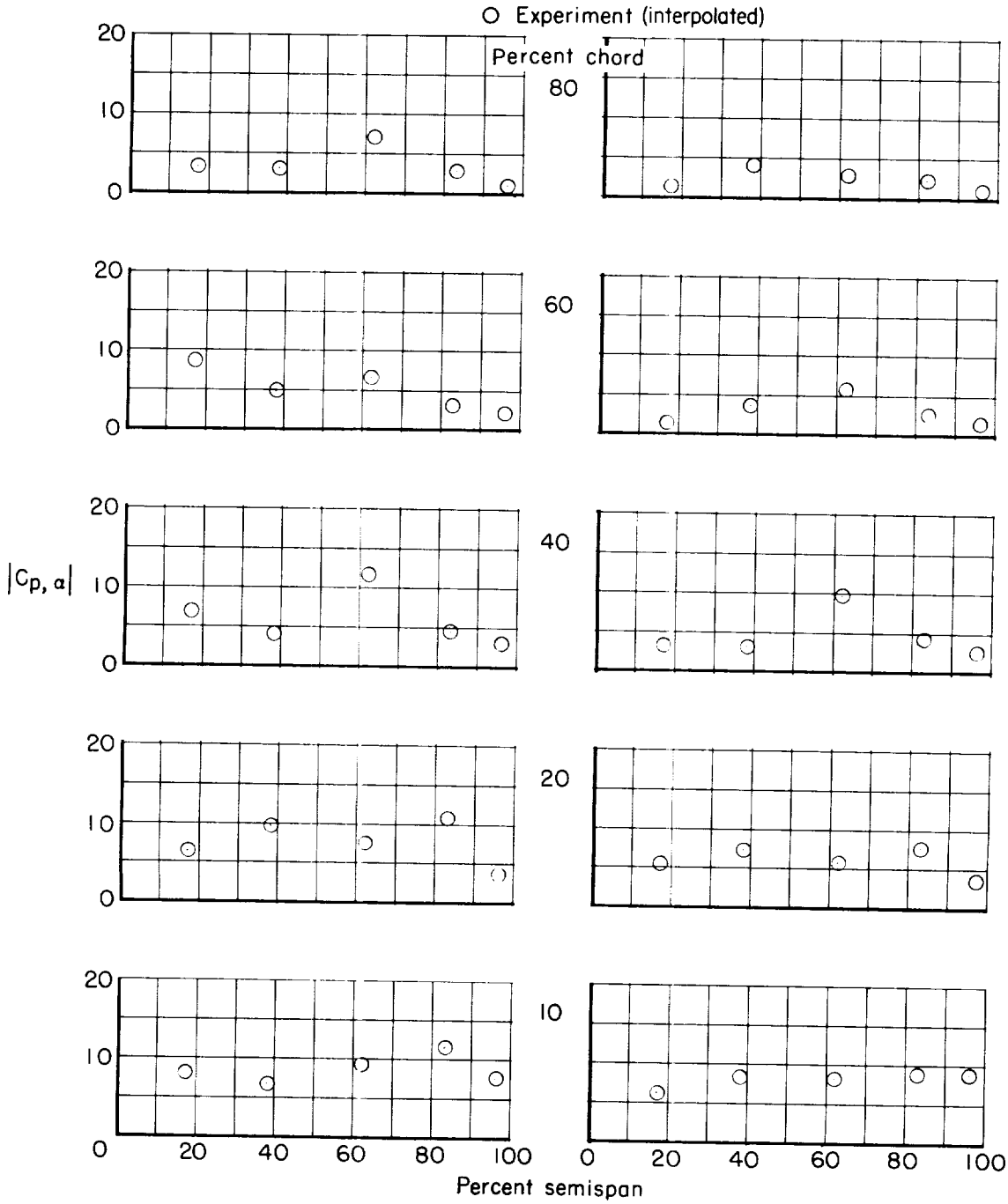

(e) Pressure coefficient for M = 0.95.

(f) Pressure coefficient for M = 1.05.

Figure 11.- Concluded.

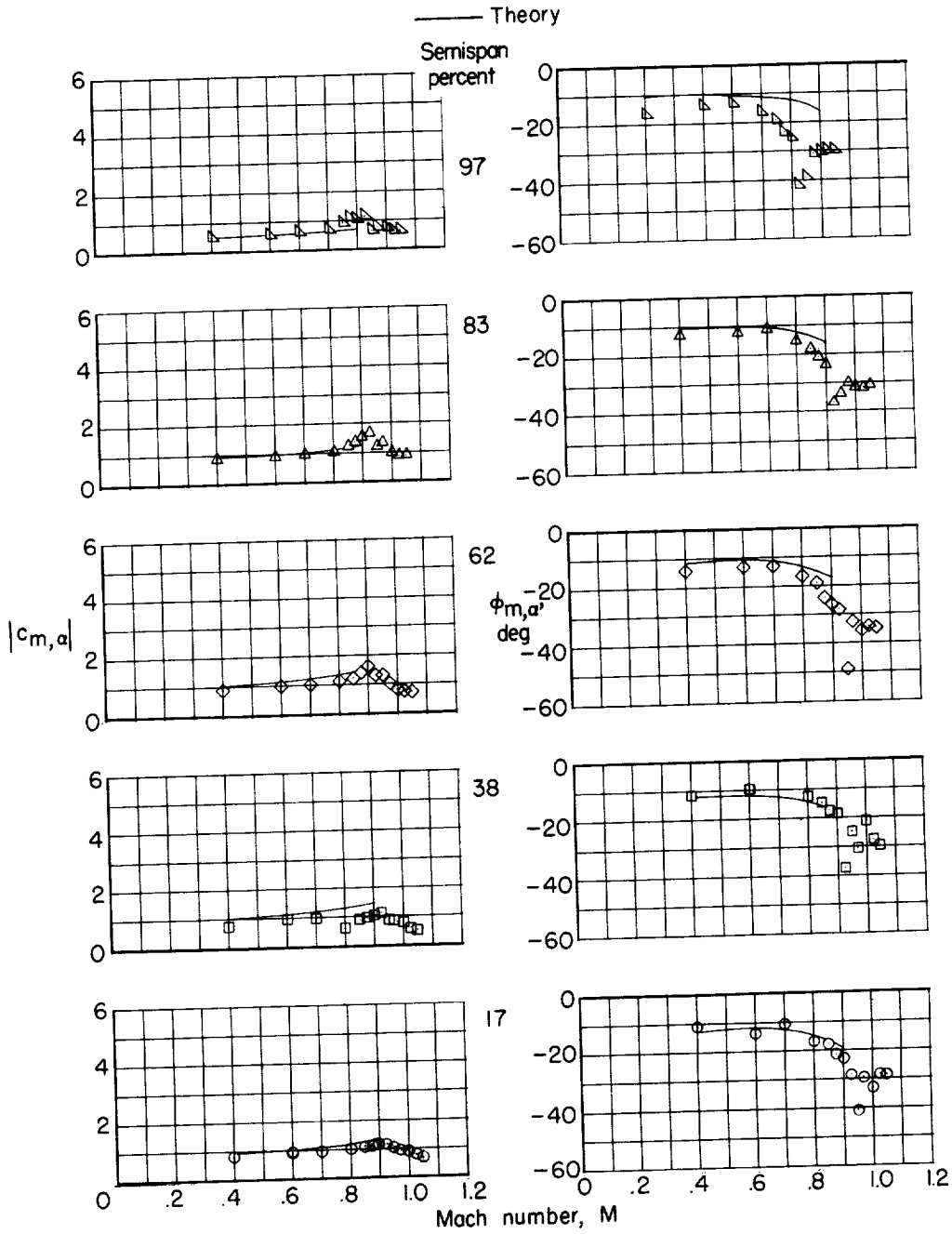

(a) Pitching-moment coefficient for $\alpha_m = 0^\circ$.

(b) Phase angle for $\alpha_m = 0^\circ$.

Figure 12.- Variation of section pitching-moment coefficient and phase angle with Mach number.

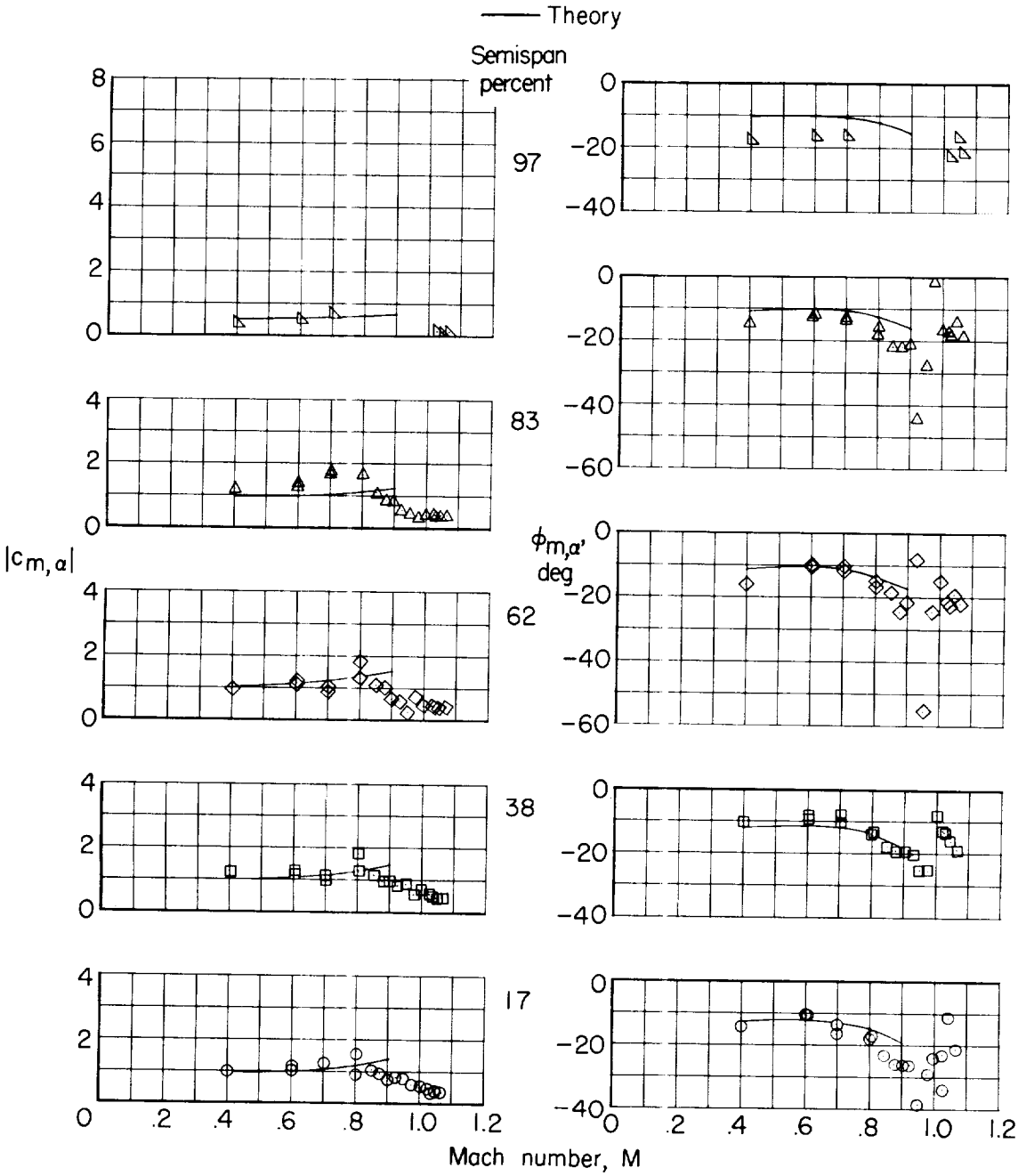

(c) Pitching-moment coefficient for $\alpha_m = 5^\circ$.

(d) Phase angle for $\alpha_m = 5^\circ$.

Figure 12.- Continued.

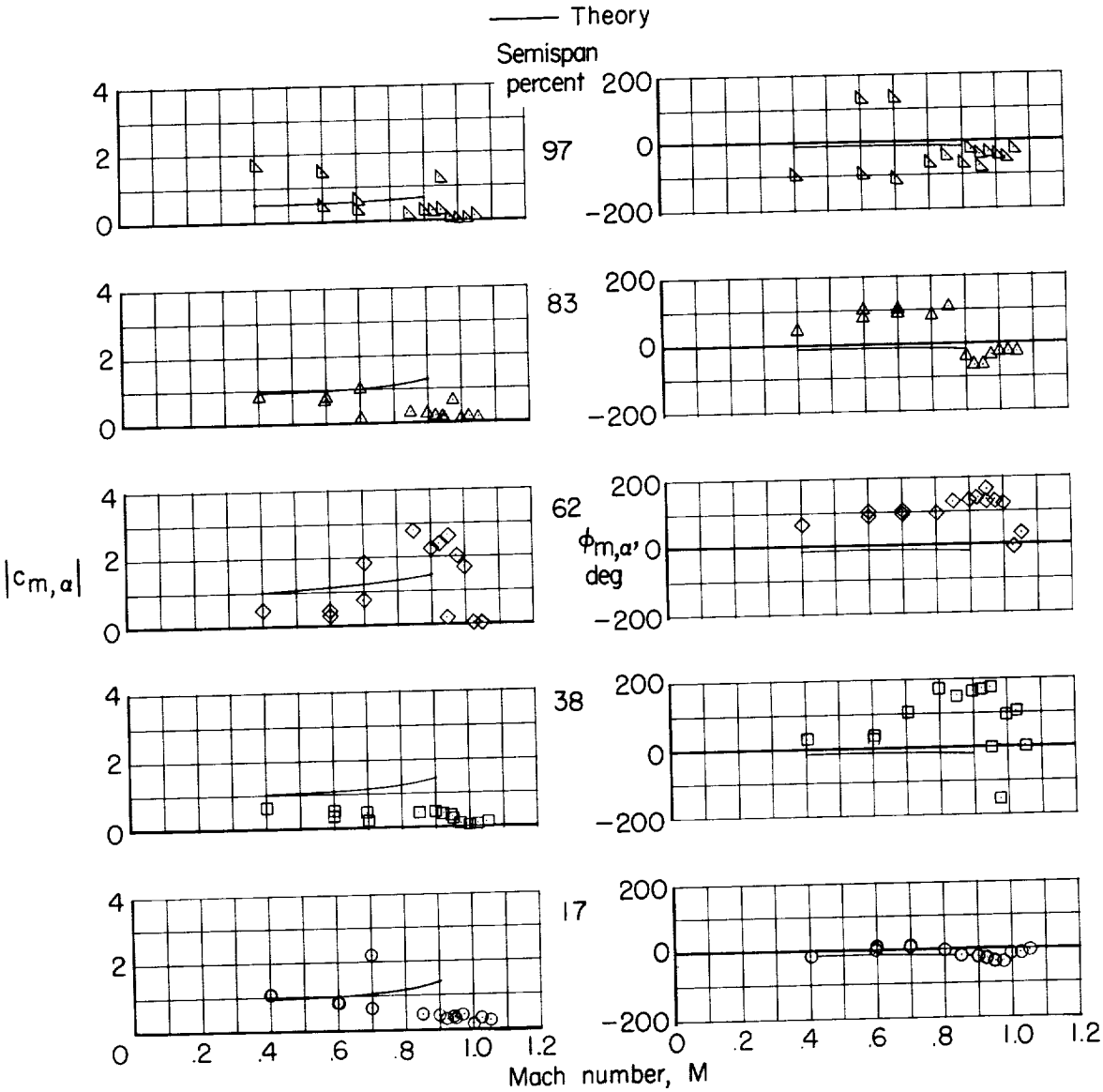

(e) Pitching-moment coefficient for $\alpha_m = 10^\circ$.

(f) Phase angle for $\alpha_m = 10^\circ$.

Figure 12.- Concluded.

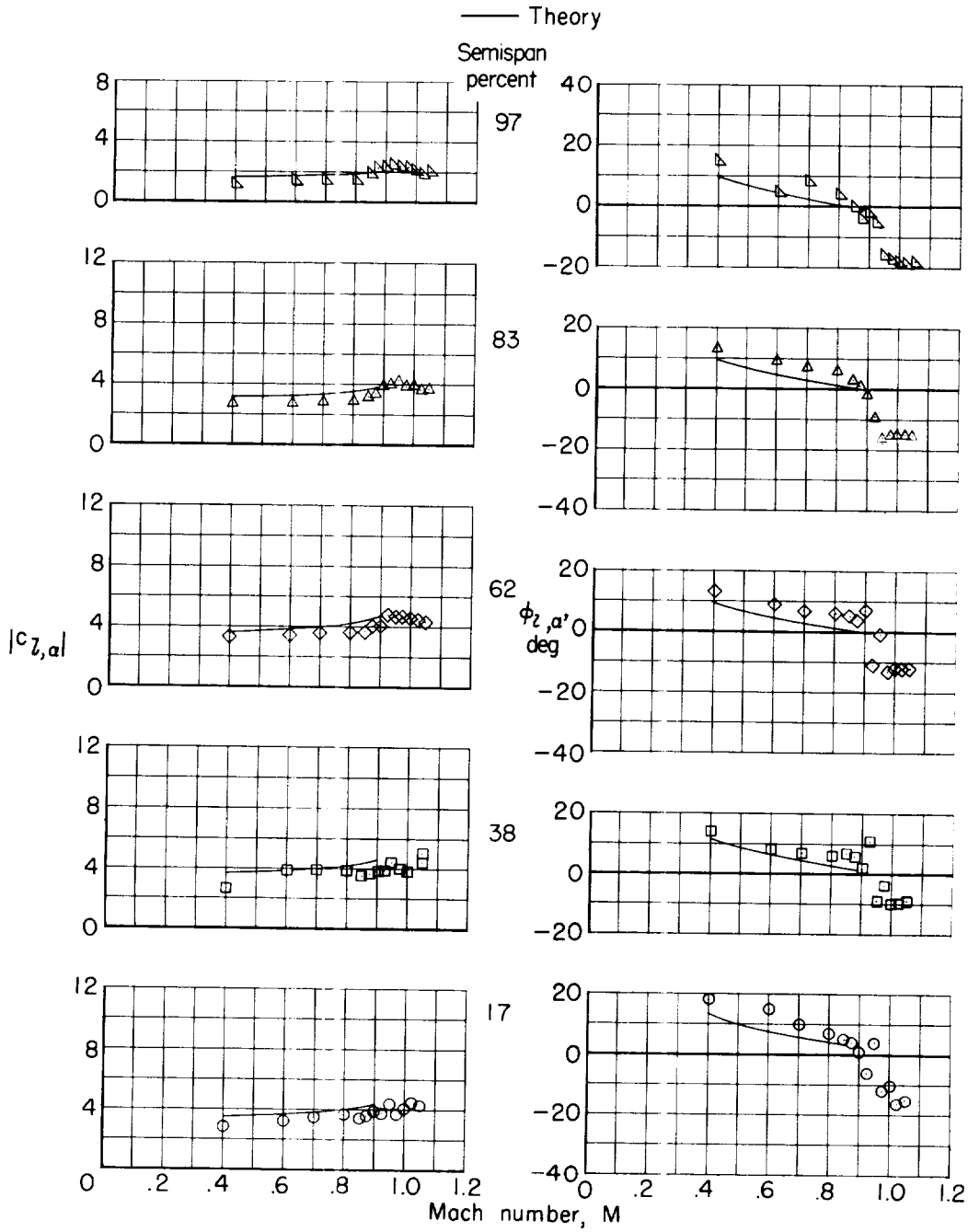

(a) Lift coefficient for $\alpha_m = 0^\circ$. (b) Phase angle for $\alpha_m = 0^\circ$.

Figure 13.- Variation of section lift coefficient and phase angle with Mach number.

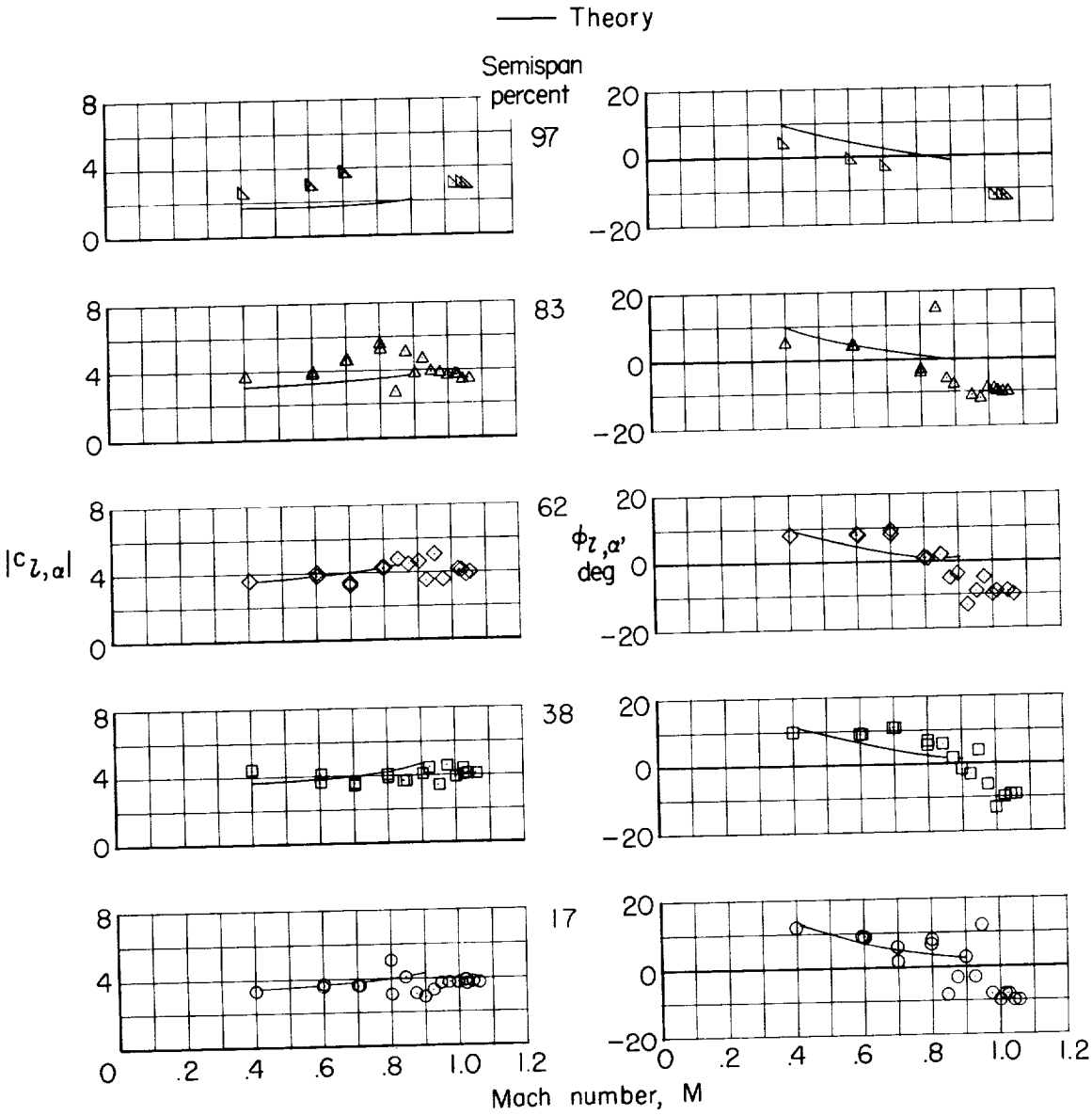

(c) Lift coefficient for $\alpha_m = 5^\circ$. (d) Phase angle for $\alpha_m = 5^\circ$.

Figure 13.- Continued.

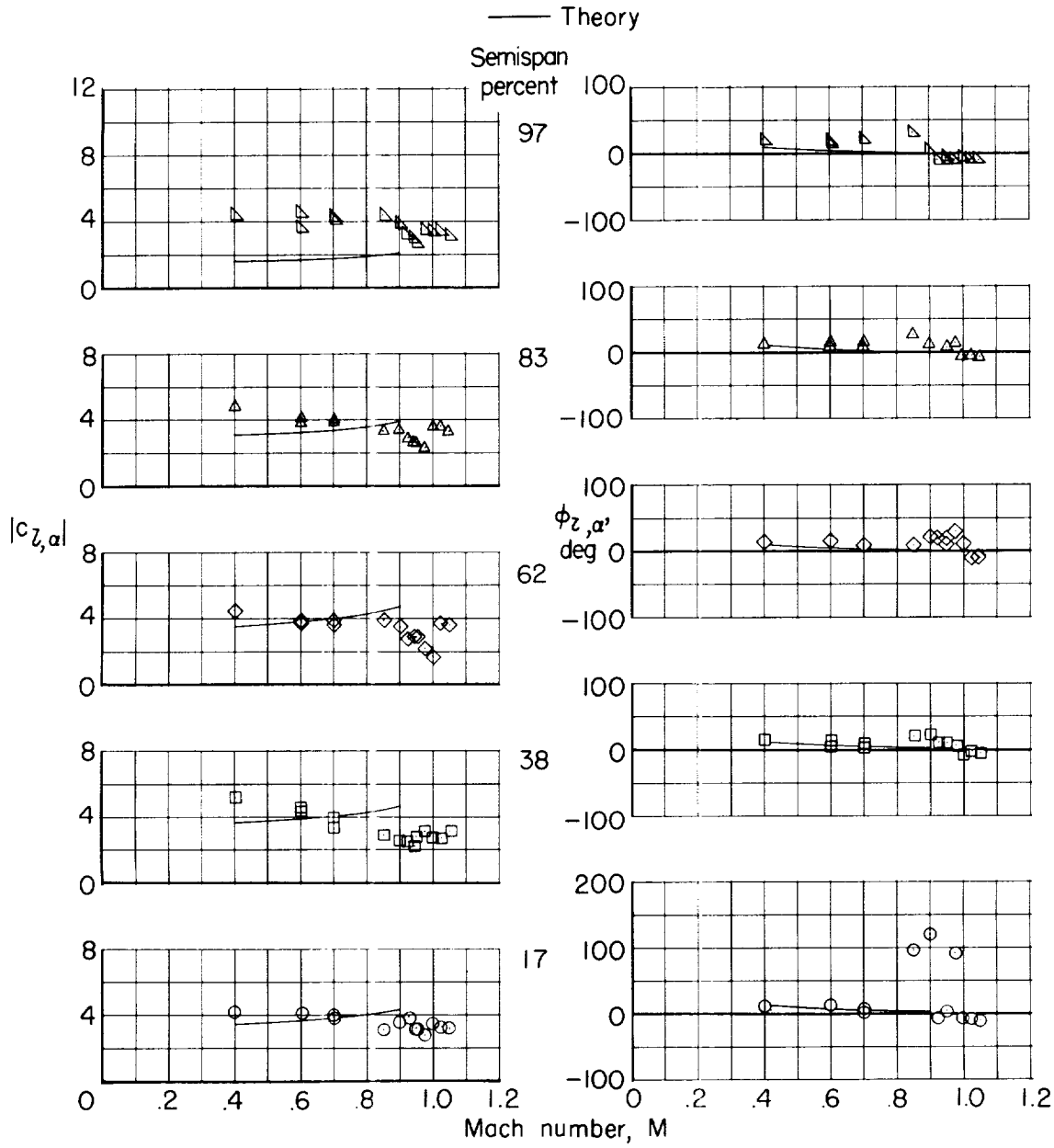

(e) Lift coefficient for $\alpha_m = 10^\circ$. (f) Phase angle for $\alpha_m = 10^\circ$.

Figure 13.- Concluded.

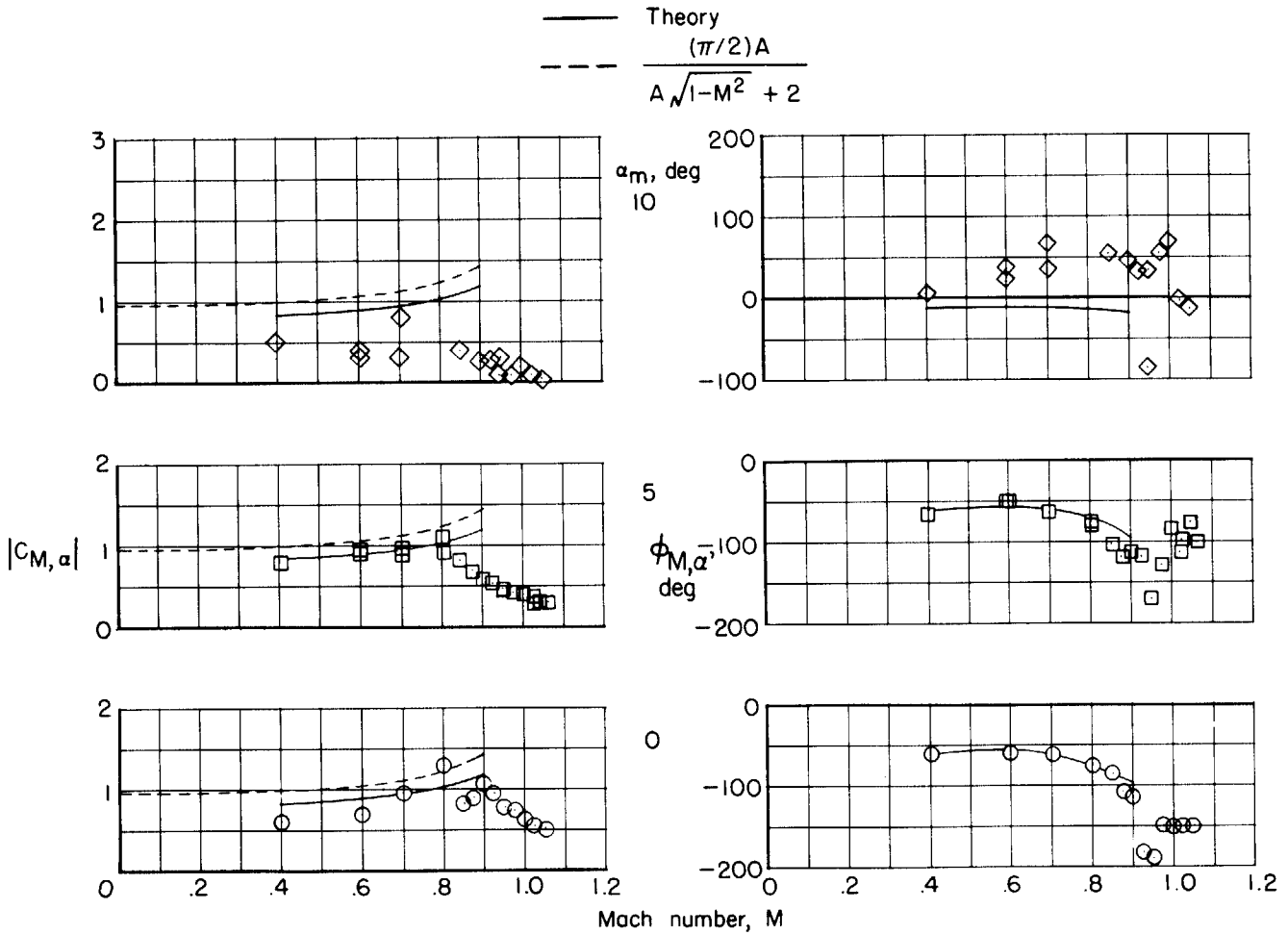

(a) Pitching-moment coefficient for $\alpha_m = 0^\circ$, 5°, and 10°.

(b) Phase angle for $\alpha_m = 0^\circ$, 5°, and 10°.

Figure 14.- Variation of total pitching-moment coefficient and phase angle with Mach number.

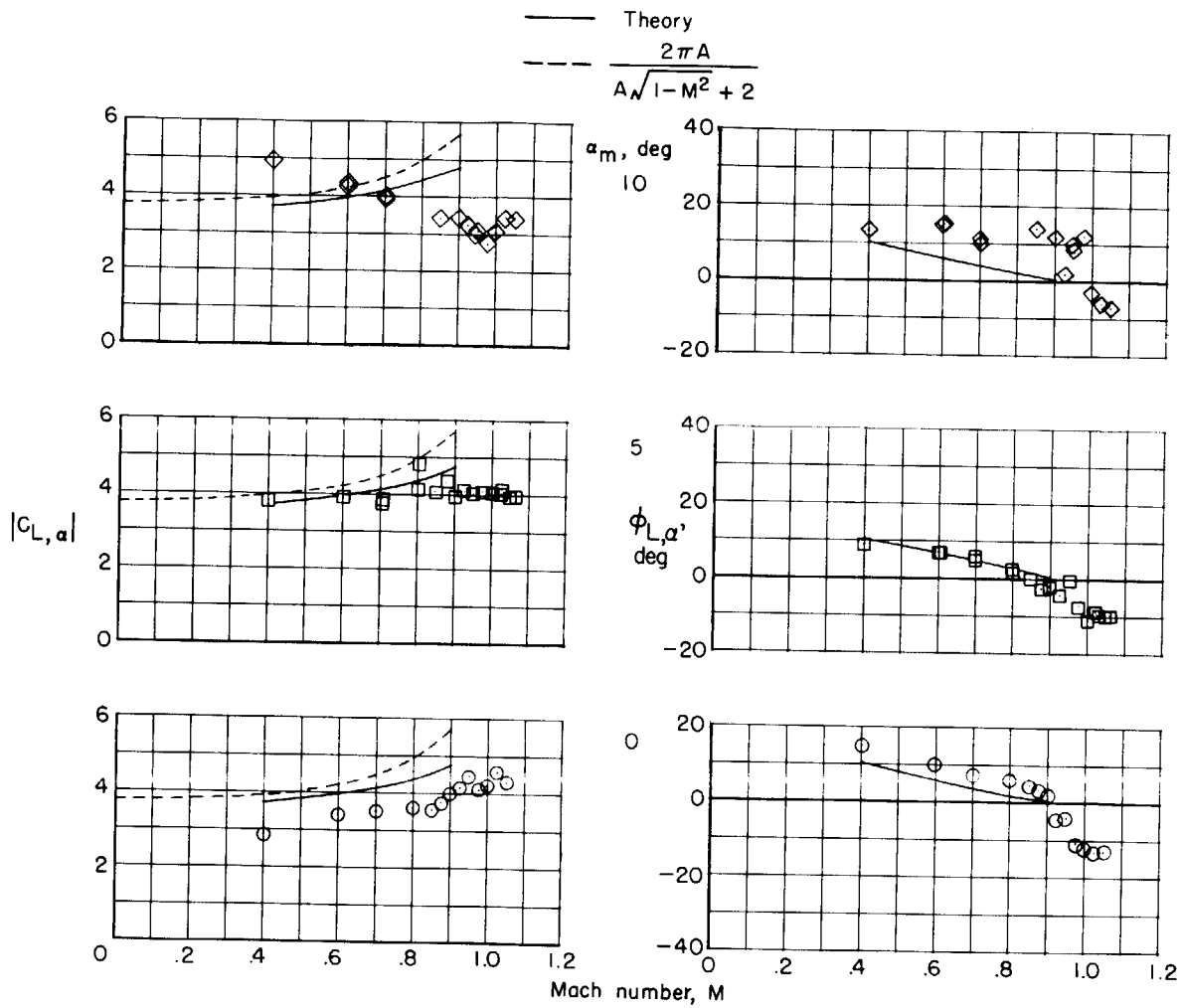

(a) Lift coefficient for $\alpha_m = 0^\circ$, 5°, and 10°. (b) Phase angle for $\alpha_m = 0^\circ$, 5°, and 10°.

Figure 15.- Variation of total lift coefficient and phase angle with Mach number.